ELECTRICAL AND MAGNETIC PROPERTIES

OF HOLMIUM SINGLE CRYSTALS

by

Donald Lawrence Strandburg

A Dissertation Submitted to the

Graduate Faculty in Partial Fulfillment of

The Requirements for the Degree of

DOCTOR OF PHILOSOPHY

Major Subject: Physics

Approved:

Signature was redacted for privacy.

In Charge of Major Work

Signature was redacted for privacy.

Head of Major Department

Signature was redacted for privacy.

Dean of Graduate College

Iowa State University
Of Science and Technology
Ames, Iowa

1961

TABLE OF CONTENTS

I. INTRODUCTION

The availability of pure rare earth metals at the Ames Laboratory has resulted in an extensive and intensive program of research aimed at the achievement of a better understanding of the fundamental properties of these metals. A summary of the experimental results up to 1956, based primarily on work done on polycrystalline materials at the Ames Laboratory, has been given by Spedding, et al. (1). The purpose of the present investigation has been to further this program of research by studying the low temperature magnetic and electrical resistivity properties of single crystals of the rare earth metal holmium.

The interesting properties of the rare earth metals are a result of their unusual electron configuration. The electron shells through the 4d are filled. The $5d^1$ and $6s^2$ electrons serve as conduction electrons in the metal, and the filled 5s and 5p shells serve as a screen for the 4f shell electrons which are responsible for the unique magnetic and electrical resistivity properties.

Holmium, which occurs in the last half of the rare earth group, has ten electrons in the 4f shell. The normal spectroscopic state has been given by Van Vleck (2) as $^5I_8$. The Landé g factor is 5/4, while S = 2, L = 6, and J = 8.

Rhodes (3) has listed most of the early measurements of the properties of the rare earths which were made on salts

rather than pure metals. Joos (4) has pointed out the differences which may occur between measurements on salts and on pure metal rare earths; consequently, only the latter work on pure metals will be presented.

Herrmann, et al. (5) have determined the crystal structure and lattice constants for holmium at room temperature. They found that the metal has the hexagonal close-packed structure. Neutron diffraction measurements of Koehler[1] have shown no change of crystal structure down to liquid helium temperatures.

Colvin, et al. (6) measured the electrical resistivity of polycrystalline holmium from $1.4°K$ to $300°K$. The resistivity versus temperature curve showed a change of slope at $19°K$ and a small peak at $127°K$. Their data are included in Figure 20 of this report.

Specific heat measurements from $12°K$ to $300°K$ on polycrystalline holmium by Gerstein, et al. (7) revealed two anomalous regions. A small peak occurred at $19.4°K$, and a much larger one occurred at $131.6°K$. The details of the curve just below the peak at $131.6°K$ have not been completely determined, and some irregularity exists in this region.

Measurements of thermoelectric power of polycrystalline rare earth metals at temperatures from $70°K$ to $300°K$ have been made by Lorn (8). He reports that the graph of thermoelectric

---

[1]Koehler, W. C. Oak Ridge National Laboratory, Oak Ridge, Tenn. Concerning neutron diffraction data on holmium. Private communication. (1960).

power versus temperature shows a sharp change in slope near 130°K, but that there is little indication of the transition near 20°K which was observed in resistivity and specific heat measurements.

Rhodes, et al. (9) have measured the magnetic properties of polycrystalline holmium from 4.2°K to 300°K. Paramagnetic and antiferromagnetic behavior were observed, and the Néel temperature was estimated to be 133°K. Remanance and magnetic hysteresis were observed at 4.2°K. A paramagnetic Curie temperature of 85°K and an effective paramagnetic Bohr magneton number of 10.9 were determined. The approach of the magnetic moment to saturation was observed to follow a $T^{3/2}$ law, and an absolute saturation moment of 310 cgs units per gram was obtained.

Recent measurements on a series of rare earth metal samples have indicated that it is extremely difficult to obtain truly polycrystalline samples, as the rare earth metals tend to form solids having a preferred direction of crystal orientation. It is clearly quite difficult to obtain meaningful data from samples composed of crystals which are partially aligned. Results reported from measurements on polycrystalline material should therefore be studied to determine whether special efforts have been made to obtain specimens having randomly oriented crystals. The degree of success of these efforts and the effect which partial

orientation would have on the data should be considered.

A program is being carried out at this laboratory to obtain single crystals of the rare earth metals and measure their properties. Behrendt, et al. (10, 11) have measured the magnetic properties of single crystals of the rare earth metals neodymium and dysprosium, while Green, et al. (12) have measured the magnetic and electrical resistivity properties of single crystals of erbium. Hall, et al. (13, 14) have made electrical resistivity measurements on yttrium and dysprosium single crystals.

Measurements on single crystals should give unique sets of data from which the behavior of polycrystalline samples may be predicted by the use of suitable averaging processes. Of greater importance, however, is the fact that single crystal data are required for the development of more precise theoretical explanations of the fundamental properties of matter.

II. BASIC CONCEPTS AND EQUATIONS

A. Magnetic Measurements

When a sample of material is placed in a magnetic field, H, a magnetic moment per gram, σ, results. The moment is related to the applied field by the relationship

$$\sigma_i = (X_g)_{ij} H_j \qquad (2.1)$$

The magnetic susceptibility, X_g, is a tensor in anisotropic substances such as the holmium single crystals used in this investigation. Measurements of σ for H directed along the a- and c-axes and the $\langle 10\bar{1}0 \rangle$ direction of the hexagonal crystal (these are the principal directions) will give all the terms of the susceptibility.

The sign, magnitude, and temperature variation of X_g may be used to group the magnetic properties of materials into three classifications:

(1) diamagnetism

(2) paramagnetism

(3) ferromagnetism, antiferromagnetism, ferrimagnetism

A review of the development of the theory of magnetism has been given by Van Vleck (15).

X_g is negative, small and nearly temperature independent for diamagnetism. All atoms or ions having closed electronic shells exhibit a diamagnetic term in their total suscepti-bility [see Dekker (16), p. 451]. The diamagnetic suscepti-bility of the free electrons of metals is discussed by

Wilson (17, p. 160).

X_g is positive, small and usually temperature dependent
for paramagnetism. Permanent magnetic dipoles exist in
paramagnetic materials, and the magnetic moment per gram, σ,
results from the partial alignment of the dipoles with the
applied magnetic field.

Many metals display a weak paramagnetism which is due to
their conduction electrons. Conduction electrons, because
of their spin, have a permanent magnetic moment of very close
to one Bohr magneton. The Bohr magneton, μ_B, is defined as

$$\mu_B = \frac{eh}{4\pi mc} \qquad (2.2)$$

where e is the electronic charge, m is the electronic mass, c
is the velocity of light, and h is Planck's constant. The
paramagnetic contribution of conduction electrons to the
susceptibility is properly calculated using Fermi-Dirac
statistics. Ordinary classical statistics leads to a value
which is too high. The correct statistical treatment gives a
paramagnetic term which is generally quite small and nearly
temperature independent. Wilson (17, p. 150) discusses this
term and shows that it is approximately three times as large
as the diamagnetic contribution of nearly free conduction
electrons.

Substances exhibiting strong paramagnetism have ions with
permanent magnetic moments. Experimentally, the magnetic
susceptibility for this case follows the Curie law,

$X_g = \frac{C_g}{T}$, or the Curie-Weiss law, $X_g = \frac{C_g}{T-\Theta_p}$, where C_g is the

Curie constant per gram, Θ_p is the paramagnetic Curie temperature and T is the absolute temperature.

The magnetic susceptibilities for substances with the properties listed in group three are positive, often large, and are field as well as temperature dependent. The permanent magnetic moments of these substances are linked by relatively strong interactions which will be discussed later.

According to quantum theory, the permanent magnetic moments of paramagnetic ions are due to the existence of a nonzero value of the total angular momentum, J, in the ground state. There are 2J + 1 possible components, m_A, of the magnetic moment per atom along the direction of an applied field:

$$m_A = M_J g \mu_B \text{ where } M_J = J, (J-1), \ldots,$$
$$-(J-1), -J. \tag{2.3}$$

M_J is the magnetic quantum number, μ_B is the Bohr magneton, and g is the Landé g factor

$$g = 1 + \frac{J(J+1) - L(L+1) + S(S+1)}{2J(J+1)}. \tag{2.4}$$

For a substance having $\frac{N_o}{A}$ ions per gram, which is placed in a magnetic field H, the application of statistical mechanics gives a resultant magnetic moment per gram, σ, expressed by

$$\sigma = \frac{N_og}{A} \, J\mu_B \, B_J(x), \qquad (2.5)$$

where $x = \frac{gJ\mu_B H}{KT}$, N_O is Avogadro's number, A is the atomic

weight, and $B_J(x)$ is the Brillouin function defined by

$$B_J(x) = \frac{2J+1}{2J} \coth\left[\frac{(2J+1)x}{2J}\right] - \frac{1}{2J} \coth\left[\frac{x}{2J}\right]. \qquad (2.6)$$

For high temperatures and low fields where $x \ll 1$, Equation

2.4 may be written as

$$\sigma = \frac{N_oJ \, (J+1)g^2\mu_b H}{A \, 3KT}, \qquad (2.7)$$

or $\quad \frac{\sigma}{H} = X_g = \frac{N_oJ \, (J+1)g^2\mu_B^2}{A \, 3KT}. \qquad (2.8)$

This is seen to be the Curie law with the Curie constant, C_g,

given by

$$C_g = \frac{N_oJ \, (J+1) \, g^2\mu_B^2}{A3K}. \qquad (2.9)$$

In order to explain the behavior of ferromagnetic

substances, which follow the Curie-Weiss law at sufficiently

high temperatures and show cooperative effects at lower

temperatures, Weiss (18) proposed that the molecular magnetic

field acting on a given dipole moment is actually

$$H_m = H + \gamma \sigma. \qquad (2.10)$$

H is the applied field, σ is the magnetic moment per gram, and

γ is a molecular field constant.

The calculations of Weiss were made using the classical

theory of Langevin (19) which considered freely rotating

dipoles. The concept of the molecular field may be used

equally as well in quantum theory. When one substitutes

Equation 2.10 into Equation 2.7 and solves for $\dfrac{\sigma}{H}$, the following result is obtained:

$$\frac{\sigma}{H} = X_g = \frac{C_g}{T - \Theta p} \; . \tag{2.11}$$

This is seen to be the Curie-Weiss law. In this equation Θp, the paramagnetic Curie temperature, equals γC_g; and

$$C_g = \frac{N_O}{A} \frac{J\,(J+1)}{3K} g^2 \mu_B{}^2 \tag{2.12}$$

which is the same as Equation 2.9.

The effective paramagnetic moment is defined as

$$\mu_{eff} = g \left[J\,(J+1) \right]^{1/2} \; . \tag{2.13}$$

It represents the total magnetic moment per ion associated with J and is expressed in Bohr magnetons. Upon substituting Equation 2.13 into Equation 2.12 and solving for μ_{eff}, one obtains

$$\mu_{eff} = \left(\frac{3KAC_g}{N_O \mu_B{}^2} \right)^{1/2} \mu_B = 2.83 \sqrt{AC_g} \; . \tag{2.14}$$

The value of the saturation magnetization for a ferromagnetic substance may be obtained from Equation 2.5 by considering the limit of large $\dfrac{H}{T}$. In this case $B_J(x) \rightarrow 1$ and

$$\sigma_{sat} = \frac{N_O}{A} g\, J \mu_B \tag{2.15}$$

or $\quad N_{eff} = g\, J \; . \tag{2.16}$

N_{eff} is the number of Bohr magnetons contributed by each ion to the saturation magnetization.

A discussion, based on the Weiss molecular field, of the

spontaneous magnetization which appears in ferromagnetic substances below the Curie temperature is given by Dekker (16, p. 466).

Estimations of the required magnitude of the Weiss molecular field show that its origin cannot be found in ordinary magnetic dipole-dipole interactions. Heisenberg (20) showed that the large molecular field could be explained in terms of the electrostatic interaction between electrons of different ions. This so-called exchange interaction between two atoms, i and j, may be represented in the potential energy as a direct coupling between total spins by a term

$$V_{ij} = - 2 J_{ij} \vec{S}_i \cdot \vec{S}_j \qquad (2.17)$$

where J_{ij} is the exchange integral for the two atoms, and $\vec{S}_i$ and $\vec{S}_j$ are the total spin angular momentum vectors for atoms i and j. Clearly, in order for the coupling between the spins to be ferromagnetic, the sign of the exchange integral must be positive.

The Heisenberg theory of ferromagnetism is seen to be based upon a description of localized spins and atomic-type wave functions. Criticism has been raised that this could not represent the true conditions in a metal, and Wilson (17, p. 182) discusses the band theory of ferromagnetism as presented by Stoner (21). An important result of Stoner's treatment is the prediction that the approach of the magnetic

moment to saturation will be proportional to T^2. Because the
4f shell of the rare earths is well shielded by outer filled
shells, however, a treatment of the magnetic properties in
terms of localized spins as in the Heisenberg theory seems to
be more appropriate.

A substance which has an antiferromagnetic state is
characterized by a magnetic susceptibility which has a peak
at some temperature called the Neel point. At temperatures
above the Néel point, the substance behaves paramagnetically,
with the susceptibility following the Curie-Weiss law. Below
the Néel point, the ionic magnetic moments are coupled so that
the susceptibility is reduced. For rare earths, a transition
from antiferromagnetic to ferromagnetic ordering often occurs
at some lower temperature.

The theory of antiferromagnetism is usually based on a
model which requires that the ionic magnetic moments tend to
orient themselves antiparallel to one another. It can be
seen from Equation 2.16 that a negative exchange integral
would lead to this type of antiferromagnetic alignment. A
substance is then ferromagnetic or antiferromagnetic depending
on whether the exchange integral is positive or negative.

Zener (22) has suggested that a change from a ferro-
magnetic to an antiferromagnetic state need not require a
change in the sign of the exchange integral, however. He
postulates two competing exchange forces. The 4f shells of

adjacent ions are coupled directly by an antiferromagnetic
exchange. They are also coupled by an antiferromagnetic
exchange to the spins of the conduction electrons. The ion-
conduction electron coupling leads to an indirect ferromag-
netic coupling between the spins of the ions. The substance
will then be ferromagnetic or antiferromagnetic depending upon
which type of coupling is stronger.

Kasuya (23), in a spin wave treatment, has used Zener's
concept of interaction between incomplete inner shell elec-
trons and conduction electrons to explain the appearance of
ferromagnetic and antiferromagnetic behavior in rare earths.
In his treatment the conduction electrons are treated as
nearly free electrons having Bloch type wave functions, while
the 4f electrons are considered as localized and having non-
overlapping atomic type wave functions. Direct interactions
between unfilled shell electrons are thus disregarded. Kasuya
obtains a $T^{3/2}$ law for the temperature dependence of the
approach of the magnetic moment to saturation as did Bloch
(24), who first applied the spin wave theory to the treatment
of ferromagnetism. It is important to notice that Kasuya
disregarded the contribution of the orbital angular momentum
to the magnetization, so that his results hold best for
gadolinium for which L = 0. Also, his treatment of
antiferromagnetism considered the usual model in which the
crystal lattice is divided into two equivalent sublattices.

The spins in each sublattice are parallel, but the magnetizations of the two sublattices are antiparallel.

De Gennes (25) has considered the same type of coupling between magnetic spins and the conduction electrons. He shows that the paramagnetic Curie point should vary as $(g - 1)^2 J(J + 1)$ for the heavy rare earths. Neither Kasuya nor de Gennes considers single crystals and the effects of anisotropy. Miira (26), in a spin-wave calculation, has shown that the T^2 dependence of the magnetization of single crystals of dysprosium at low temperatures which was reported by Behrendt, et al. (11) may be attributed to the magnetic anisotropy.

Liu, et al. (27) discussed the antiferromagnetic behavior of dysprosium in terms of the molecular field theory. The type of antiferromagnetic ordering upon which their treatment is based is the same as that used by Kasuya.

Recently, the concept of the helical spin structure has been discussed theoretically by Yoshinori (28), Villain (29), and Koehler (30). Neutron diffraction data of Herpin and Meriel (31) have indicated the existence of the helical spin arrangement in $MnAu_2$, while Cable, et al. (32) have interpreted data from neutron diffraction measurements on single crystals of holmium, dysprosium, and erbium as resulting from a helical spin arrangement where the magnetic moments are parallel within each hexagonal layer but rotate by an angle ω

per layer in successive planes along the C axis. The angle of
rotation between successive layers varies continuously from
50° per layer at 120°K to 36° per layer near 35°K. The angle
of 36° remains constant down to near 20°K.

B. Resistivity Measurements

Great advances in the theoretical interpretation of
electrical properties of metals have been made since the
discovery of the electron by J. J. Thomson in 1897, and many
of the important features of the electrical resistivities of
metals, especially the group I metals, are rather well
explained. A complete description of the basic theory of
electron transport processes as developed by Sommerfeld,
Bloch, and others is given by Wilson (17), while Bardeen (33)
has given an excellent summary of the historical development
of the theory up to 1940. The theoretical interpretation of
experimental data becomes more difficult and incomplete when
the transition metals, the rare earths, and other polyvalent
metals are considered.

All modern theories of the motion of electrical charges
through a metal consider the passage of electrons through a
more or less ordered array of atoms. It has been shown by
Bloch (34) and Jones (35), among others [see Dekker (16,
chapter 10) for a simplified treatment] that a perfect metal
crystal having no impurities and no motion of the atoms from
their equilibrium positions will present a perfectly periodic

potential to the electron wave and will offer no resistance to its passage. Resistance is due only to imperfections in the periodicity of the potential. These imperfections arise from thermal vibration of the atoms from their equilibrium positions, (phonon scattering); aperiodicity of the magnetic moments associated with some ions, (magnon scattering), and other crystal imperfections which are classed as defects. These include foreign atoms, lattice defects, boundaries, and the presence of more than one isotope of the atoms.

According to Matthiessen's rule (36), the resistivity of a metal is separable into an ideal part, $\rho_i(T)$, which is temperature dependent and characteristic of the pure metal, and a residual part, ρ_{res}, which is temperature independent and is due to the defects discussed previously.

$$\rho = \rho_{res} + \rho_i(T) \tag{2.18}$$

Matthiessen's rule is only approximately true, and deviations from it have been discussed by MacDonald (37) and Gerritsen (38). However, the temperature variation of ρ_{res} is small compared to the value of ρ_{res} so that its temperature variation is significant only when the ideal and residual resistivities are of the same order of magnitude.

The two contributions to $\rho_i(T)$ are seen to be phonon, ρ_{ph}, and magnon, ρ_{mag}, resistivity. If one assumes that these quantities approach zero as the absolute temperature approaches zero, the residual resistivity, ρ_{res}, may be

determined by measuring the resistivity of a sample at very
low temperatures where the total resistivity, ρ , becomes
constant.

For most metals, there is no magnon contribution to the
resistivity; and the major contribution to $\rho_i(T)$ comes from
the thermal vibration of the lattice through phonon-electron
interactions. The most commonly used formula for the
temperature dependence of the phonon resistivity was
developed semi-empirically by Gruneison (39) and later
obtained from theoretical considerations by Bloch (40). A
development of the theory is also given by Wilson (18). The
formula can be expressed as

$$\rho_{ph}(T) = A\left(\frac{T}{\Theta}\right)^5 \int_0^{\frac{\Theta}{T}} \frac{x^5 dx}{(e^x-1)(1-e^{-x})} = A\left(\frac{T}{\Theta}\right)^5 F\left(\frac{\Theta}{T}\right) \quad (2.19)$$

where A is a constant characteristic of the metal and T is the
absolute temperature. A fair approximation of Θ is often
given by the Debye Θ for specific heat. The general proper-
ties of the integral in Equation 2.19 have been discussed by
Sondheimer (41) and by Wilson (18, p. 335). Limiting expres-
sions for the integral at high and low temperatures may be
obtained by the following methods.

$$\frac{\Theta}{T} \ll 1; \quad F\left(\frac{\Theta}{T}\right) = \int_0^{\frac{\Theta}{T}} \left(x^3 - \frac{x^5}{12} + \ldots\right) dx =$$

$$\frac{1}{4}\left(\frac{\Theta}{T}\right)^4 - \frac{1}{72}\left(\frac{\Theta}{T}\right)^6 + \ldots \simeq \frac{1}{4}\left(\frac{\Theta}{T}\right)^4 \quad (2.20)$$

$$\frac{\Theta}{T} \rightarrow \infty \; ; \; F\left(\frac{\Theta}{T}\right) = 5 \int_0^\infty \frac{x^4 dx}{e^x - 1} = 5! \sum_{S=1}^\infty \frac{1}{S^5}$$

$$= 124.4 \; . \hspace{3cm} (2.21)$$

Applying these results to Equation 2.19, one sees that at low temperatures ρ_{ph} is proportional to T^5, while at high temperatures ρ_{ph} is proportional to T.

Equation 2.19 has been found to give a good description of the experimental data of many metals, especially those of group I; but it is often necessary to use values of Θ which are quite different from those which fit specific heat data. A discussion of Θ values for the resistance of metals has been given by Blackman (42). MacDonald and Mendelssohn (43) have made detailed measurements of the electrical resistivity of alkali metals at low temperatures, and they treat deviations from Equation 2.19 by considering Θ as a function of T. For many metals, especially those of group I, Θ is a slowly varying function of T; and Equation 2.19 gives a useful interpretation of the data. However, for other metals, for example the transition metals, $\Theta(T)$ varies so widely that calculations based on Equation 2.19 are meaningless and explanations of the phenomena involved must be sought along other lines.

Mott (44), in considering the relatively high resistivity of the transition elements, proposed a two-band model where most of the current is carried by almost-free s-band electrons.

These electrons may be scattered by phonons into holes in the d-band which has a much lower Fermi velocity so that an increase in resistivity results from the transition. Since the d-electrons are responsible for the magnetic properties of the transition metals, Mott also considered the effects of magnetic ordering upon the s-d interaction. Using this interaction concept, Wilson (45) showed that the s-d interaction would give an additional contribution to ρ_{ph} of Equation 2 that would vary as T^3 at low temperatures. However, Ziman (46) has commented that lack of knowledge of the actual shape of the Fermi surface makes it impossible to arrive at the exact power law for the resistivity. White and Woods (47) have measured the electrical resistivity of transition elements from 295°K to 10°K, and at low temperatures they find that $\rho_i \propto T^m$ where m ranges from 3 to 5.

Anomalous effects in the resistivities of ferromagnetic and antiferromagnetic materials have been attributed to spin-wave or magnon scattering of conduction electrons. Kasuya (48) and de Gennes and Friedel (49) have assumed that the contribution of magnon scattering to the resistivity, ρ_{mag}, is additive to the contributions of phonon scattering, ρ_{ph}, and the impurity scattering, ρ_{res}, so that

$$\rho = \rho_{res} + \rho_{ph} + \rho_{mag} . \tag{2.22}$$

The contribution of magnon scattering to the electrical resistivity can be larger than the contribution of phonon

scattering at ordinary temperatures. At low temperatures the atomic moments are all aligned so that ρ_{mag} goes to zero, while at temperatures above the highest magnetic ordering temperature the spins are randomly oriented and ρ_{mag} is constant.

Electrical resistivity measurements on nickel and iron have given low temperature variations of ρ_{mag} which agree with formulas having terms in T, T^2 and T^3 (50, 51). The T term is attributed to magnon scattering.

Kasuya, in discussing the rare earths, has stated that the anomalous resistance is not due to the type of s-d interaction proposed by Mott where an s-band and d-band transition is considered. He states:

> "The resistance caused by this process should be nearly proportional to the absolute temperature in high temperatures because this process occurs through the interaction with phonons. Such a temperature dependence, however, does not seem to explain the experimental facts of the anomalous electrical resistance. It rather corresponds to the normal one."

The papers of Kasuya and de Gennes and Friedel consider the conduction electrons (s-electrons for the transition metals and s- and d-electrons for the rare earths) as nearly free as in Mott's description, while the inner shell electrons (d-electrons for the transition metals and f-electrons for the rare earths) are localized and correspond to the Heisenberg model of ferromagnetism. Since the magnetic properties of the rare earths are best described in terms of

localized magnetic moments, this model for the anomalous
resistivity seems quite plausible. It should be noted,
however, that neither development takes into consideration
the contribution of the orbital moment, so that the results
are strictly applicable only to the case of gadolinium which
has no orbital moment.

The possible anisotropy of electrical resistivity due to
the lattice structure of the crystal has been considered by
Boas and Mackenzie (52) and by Baroody (53). Boas and
Mackenzie showed that for a hexagonal crystal there would be
no anisotropy in the basal plane for any property which
represents a linear relationship between two vectors. The
conductivity is the property which relates the current vector
and the applied electric field vector. Therefore when the
relation is linear, the conductivity and the resistivity
should be isotropic in the basal plane. Since the magnetic
susceptibility also gives the relationship between two vectors,
magnetic anisotropy should appear in the basal plane only when
the relationship is no longer a linear one.

The treatments given above have not considered the
magnetic contribution to the anisotropy, however, and the
results of rare earth single crystal measurements indicate
that this is the most important effect.

III. MATERIALS TESTED

A. Preparation of Single Crystals

Holmium has the hexagonal close-packed structure. In order that its electrical and magnetic properties might be investigated in the principal crystalline directions, it was necessary to prepare single crystals oriented along the c-axis, along the a-axis, and in a direction halfway between two a-axes in the basal plane which, in accordance with standard crystallographic notation, is called the $\langle 10\bar{1}0 \rangle$ direction.

The distilled holmium metal from which the single crystals were grown was prepared at this laboratory by use of the ion exchange process for the separation of the rare earth compounds (54) and a reduction process for the preparation of the very pure metal from the flouride (55).

Single crystals were grown from the pure metal by means of a strain-anneal method which has been described by Hall, et al. (14). The crystals were prepared in cooperation with Harold Nigh, a member of Experimental Physics Group II of the Ames Laboratory. An arc-melted button approximately 0.8 cm thick, 3.1 cm in diameter, and weighing 43.3 gm was prepared. The button was cut into three pieces in order to obtain samples which would fit into the annealing furnace previously described by Behrendt (56). Two of the pieces were carefully polished and then annealed separately in an argon atmosphere. The piece from which the a- and c-axis samples were obtained

was annealed for twelve hours at 1320°C, while the piece from which the $\langle 10\bar{1}0 \rangle$ crystal was obtained was annealed for twenty-one hours at 1340°C. The resulting specimens each contained one large grain from which samples could be cut and several smaller ones. The grain structure was clearly visible on both pieces due to the thermal etching of the material, so that the orientation of the crystals and their extent were determined without chemical etching by back reflection Laue X-ray diffraction methods described by Greninger (57). It is felt that the arc-melting of the material and the subsequent extremely rapid cooling of the button when the electric arc is broken are essential to the growth technique, as attempts to grow single crystals by annealing cast samples of holmium were completely unsuccessful.

Three single crystals of different orientations were rough-cut from the annealed pieces with a jeweler's saw and then polished with emery paper into their final shape which was that of a rectangular parallelepiped. In order to remove any strain effects resulting from the process of sawing, at least one millimeter of material was removed from each face of the sample in the polishing operation. The a-axis crystal had dimensions of 1.14 mm by 0.98 mm by 10.5 mm and mass of 100.6 mg. The $\langle 10\bar{1}0 \rangle$ crystal had dimensions of 1.036 mm by 1.03 mm by 9.02 mm and mass 82.18 mg, and the c-axis had dimensions of 1.02 mm by 0.94 mm by 9.8 mm and mass of 82.40

mg. For each crystal the respective crystalline axis is parallel to the long dimension of the crystal.

B. Purity

Pieces of the annealed material cut from positions adjacent to the single crystals used in this work were examined spectrographically. The material was also analyzed prior to arc-melting.

The analysis of the material before it was arc-melted showed: Dy $\leq$ 0.04%; Er $\leq$ 0.01%; Tm $\leq$ 0.01%; Ca < 0.05%; Fe < 0.01%; Si < 0.02%; Ta < 0.1%; C, 73 ppm; N, 93 ppm. The carbon and nitrogen impurities were determined by analytical chemistry. The other determinations were made by spectrographic analysis. Since holmium is quite volatile, it was not possible to determine the oxygen content by the usual vacuum fusion analysis method.

The spectrographic analysis of the portion of the arc-melted button from which the a- and c-axis crystals were cut showed: Y < 0.01%; Dy < 0.04%; Er, 0.06%; Tm, 0.02%; Ca < 0.03%; Cr < 0.005%; Mg < 0.005%; Fe, 0.005%; Al, B, Mg, Nd, Ni, Pb, Pr, Sc, Si, Sm, Ta, Tb, W, Yb, not detected; Cu, very weak.

The spectrographic analysis of the separately annealed portion of the arc melted button from which the $\langle 10\bar{1}0 \rangle$ crystal was cut showed: Y < 0.01%; Dy < 0.04%; Er < 0.02%; Tm, 0.01%; Cr < 0.005%; Mg < 0.005%; Fe < 0.005%; Al, B, Ca, Ce, Co, Eu,

Gd, La, Lu, Mg, Nd, Ni, Pb, Pr, Sc, Si, Sm, Ta, Tb, W, Yb, not detected; Cu, faint trace.

VI. EXPERIMENTAL PROCEDURE

A. Method of Magnetic Measurements

Magnetic measurements were made using a standard version of the Faraday method (58). The magnetic material of mass m was placed in a non-uniform, horizontal magnetic field, H, which had a constant gradient, $\frac{d\,H}{d\,z}$, in the vertical direction. A magnetic moment per gram, σ_{HT}, which is a function of magnetic field and temperature, was induced in the sample; and a magnetic force acting vertically, F, was exerted on the sample.

$$F = m\ \sigma_{H,T}\ \frac{d\,H}{d\,z}.\tag{4.1}$$

The magnetic force on the sample was measured by an analytical balance as an apparent change in sample mass, ΔM, so that $\Delta Mg = F$, where g is the gravitational constant. The force equation can be rewritten

$$\sigma_{H,T} = \frac{\Delta M\ \dfrac{g}{m}}{\dfrac{d\,H}{d\,z}}\tag{4.2}$$

Since the sample holder was also slightly magnetic, it was necessary to make a set of calibration measurements over the temperature range from $1.4^\circ K$ to $300^\circ K$ using only the empty sample holder. These correction values were used to determine the magnetic force due to the sample alone.

The internal magnetic field acting on the magnetic ions

is dependent upon the shape of the sample and is given by

$$\bar{H} = \bar{H}_{ext} - N \sigma_{H,T} \, d \tag{4.3}$$

where d is the density of the material, H_{ext} is the external field, and N is the demagnetizing factor. It is possible to calculate exact values of N only for ellipsoids; and since the samples used in this investigation were rectangular parallelepipeds, it was necessary to use approximations described by Thoburn (59). These approximations are based on values given by Bozorth (60) which show that the demagnetizing factor for a cylinder is somewhat less than that for an ellipsoid having the same aspect ratio (length : diameter). The demagnetizing factors for samples used in this investigation were all near 2.0 and the maximum field correction was 680 oersteds which was subtracted from an external field of 18,000 oersteds.

The raw data were obtained as a set of isotherms. Measurements of the apparent increase in sample weight were made at a series of values of increasing magnetic field. Some data were also taken with decreasing fields in order that the magnetic hysteresis of the sample could be determined. The sample was annealed between isotherms by raising its temperature to at least 50°K. In fact, the annealing temperature for many of the low temperature isotherms was near 300°K. The temperature to which the sample was raised prior to each set of isothermal measurements is given with the experimental

results in Appendix A.

Values of $\sigma_{H,T}$ were obtained from the raw data, and isothermal curves of $\sigma_{H,T}$ versus H were plotted. From these curves, values were obtained for isofield plots of $\sigma_{H,T}$ versus T.

B. Apparatus for Magnetic Measurements

The 20 kw Weiss-type magnet used in this investigation was designed by Elliott (61) and modified by Thoburn (59). Pole pieces of the Sucksmith type provided a uniform vertical field gradient which could be varied from 0 to 550 oersteds/cm while the field varied from 0 to 18,000 oersteds.

A metal cryostat somewhat similar to one described by Henry and Dolecek (62) was designed for this work. A modified version of the heat leak chamber described by Anderson, et al. (63) was used as the basis for a temperature control system with which it was possible to maintain the temperature of the sample at any desired value from 1.4°K to 300°K.

Figure 1 shows the complete dewar system, while Figure 2 displays the details of the tail assembly of the dewar. A modified Voland "speedigram" analytical balance, reading to 0.1 mg, was used for measuring the forces exerted on the samples. The left hand pan of the balance was replaced by a long rigid quartz suspension rod which was terminated with the sample holder shown in Figure 2. A swivel at the top of the rod made it possible to rotate the sample holder for correct

Figure 1. Cryogenic system for magnetic measurements.
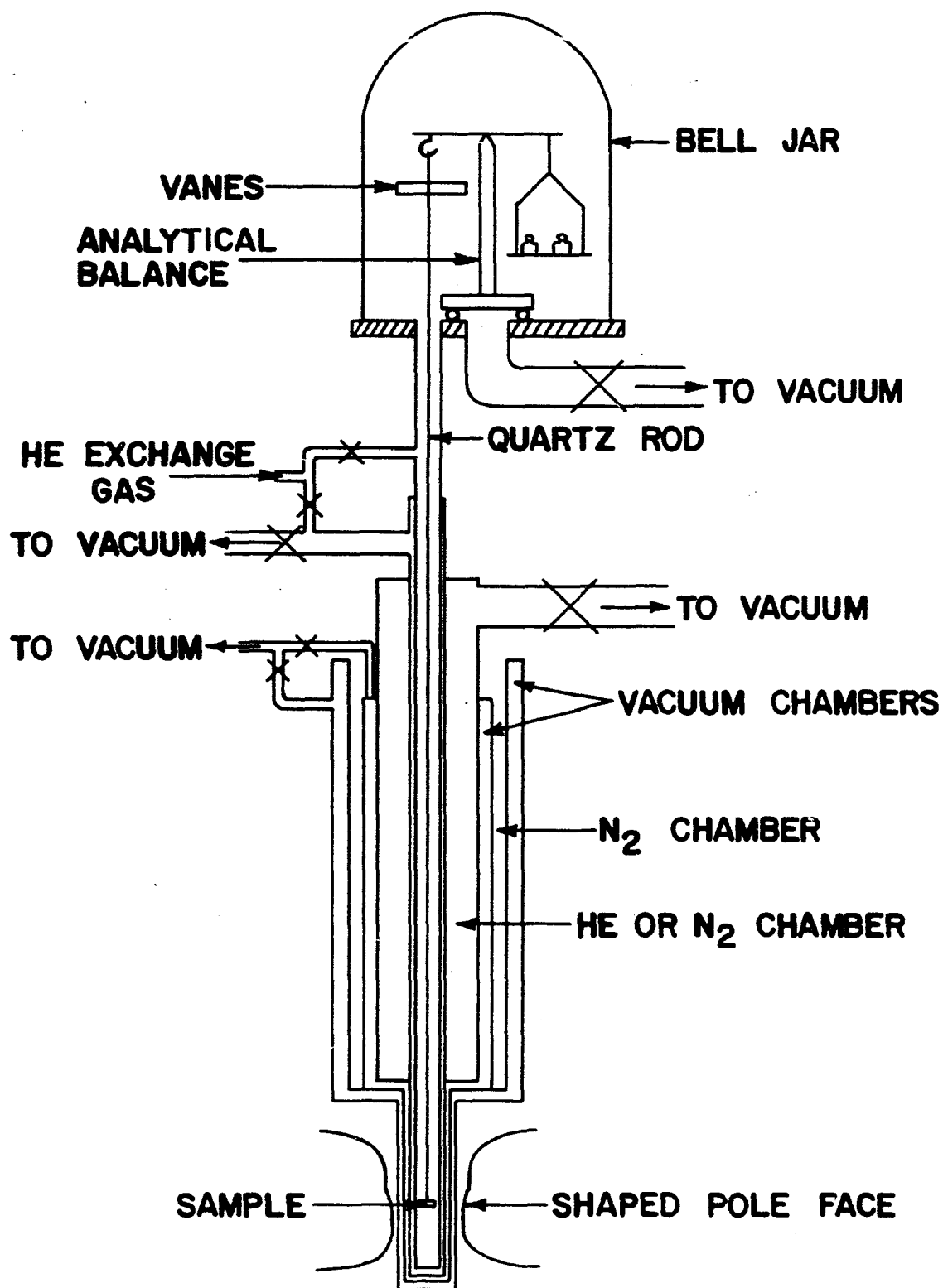
Figure 2. Details of the tail assembly of the dewar.

VACUUM

LIQUID HELIUM

LIQUID NITROGEN

COPPER SPRING CONTACT

QUARTZ ROD

A

B

C

HEATER AND COPPER TEMPERATURE MONITOR

SILK THREAD

COPPER

SAMPLE

CARBON RESISTOR-THERMOCOUPLE-TANTALUM THERMOMETER

CARBON TEMPERATURE MONITOR
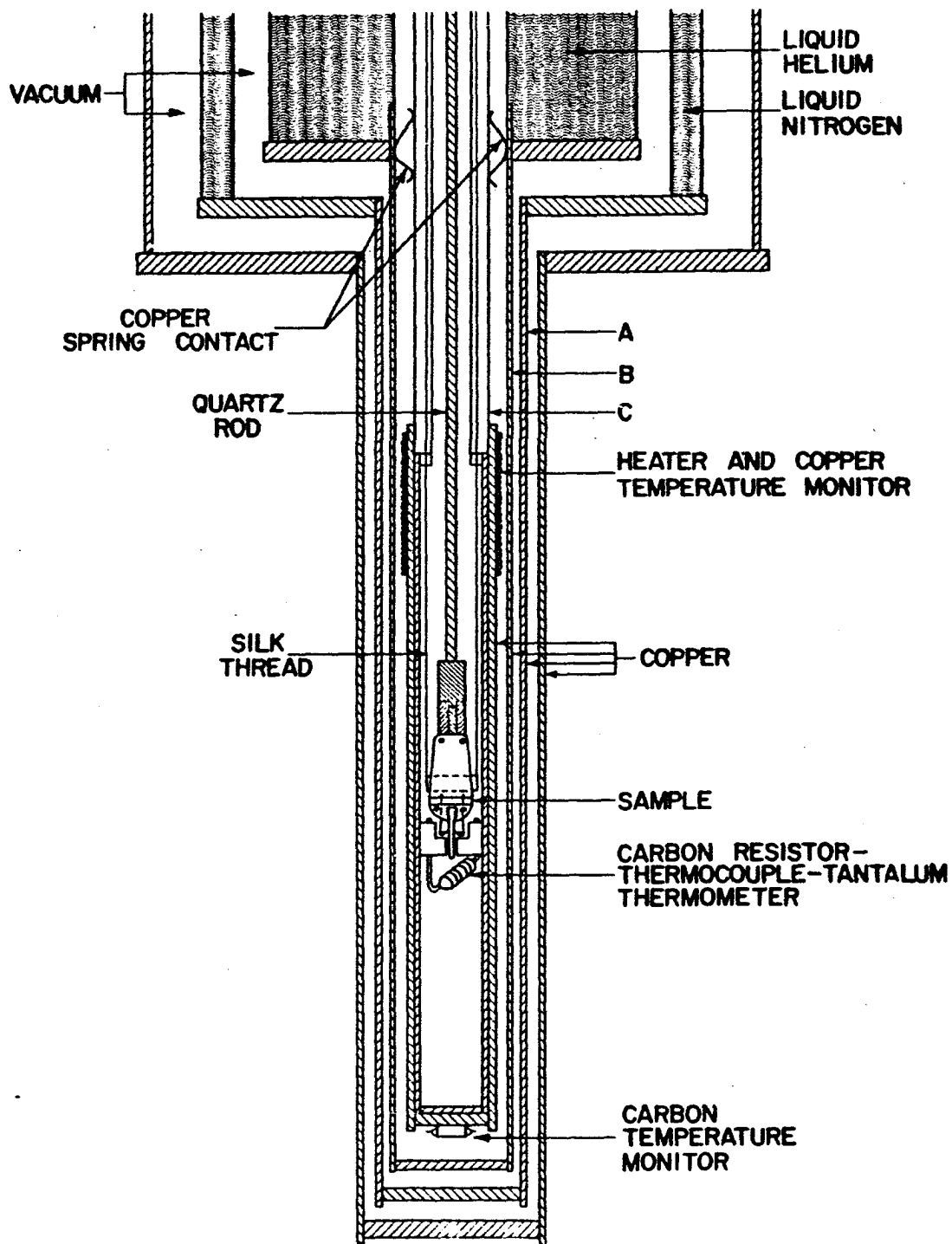
alignment of the sample.

The balance was enclosed by an eighteen inch glass bell jar, and the rotary controls of the balance were passed out of the bell jar through o-ring seals in the base plate. After the system was flushed with helium gas and then evacuated to less than one micron, helium exchange gas at a pressure of 800 to 1000 microns was introduced into the bell jar and the connecting sample chamber. This amount of exchange gas insured that the sample was in good thermal contact with the walls of the sample chamber.

In order that the closest possible spacing of the magnet pole pieces, and hence the maximum possible magnetic fields, could be obtained, the dewar was designed so that there was no refrigerating liquid in the tail assembly. A copper tube A (see Figure 2) in thermal contact with the outer liquid nitrogen chamber served as a radiation shield around an inner copper tube B which extended into the inner liquid chamber. This chamber could be filled with liquid nitrogen or liquid helium. A thin-walled non-magnetic stainless steel tube of the same diameter as tube B was silver-soldered to tube B and passed out of the inner liquid chamber through an o-ring seal at the top of the dewar. Because of its high thermal conductivity, the entire length of the copper tube B remained essentially at the temperature of the inner liquid bath.

A third tube C consisting of a long thin-walled

non-magnetic stainless steel tube with a copper tube silver-soldered to its lower end was inserted into tube B. Thermal contact was established between the stainless steel portion of tube C and the copper tube B by copper spring contacts positioned as shown in Figure 2.

Temperatures above the liquid bath temperature were obtained by evacuating the space between Tubes B and C to less than one micron and using the heater wound on the copper portion of tube C to set up a temperature gradient along the section of the stainless steel tube between the heater and the copper spring contacts. The copper contacts were positioned so that temperatures near 50°K could be maintained with a liquid helium bath by a heat input of approximately 0.1 watt.

Temperatures below the normal liquid helium bath temperature were obtained by introducing a helium exchange gas at a pressure of about 200 microns into the space between tubes B and C and reducing the pressure above the liquid coolant with a large capacity vacuum pump to lower the bath temperature and consequently the temperature of tubes B and C. The pressure above the liquid helium bath was measured with mercury and butyl phthalate manometers.

Temperatures from 1.3°K to above 80°K could be obtained with liquid helium, although the temperature range from 50°K to 77.4°K was usually covered by pumping on liquid

nitrogen. Temperatures from 77.4° to 300° were obtained through use of the heat leak chamber and liquid nitrogen.

An automatic temperature control system was used for all temperatures above 4.2°K. In order that satisfactory sensitivity might be obtained over the entire temperature range from 4.2°K to 300°K, two temperature sensing elements whose resistances are temperature dependent were used. A 51 ohm nominal resistance Allen Bradley carbon composition thermometer fastened to the bottom of tube C was used in the range from 4.2°K to 35°K. A length of copper wire having a room temperature resistance of 100 ohms was wound on top of the heater and was used in the range from 35°K to 300°K. Either element served as one arm of a Wheatstone bridge. Another arm consisted of a variable resistor which could be adjusted over the entire range of resistance values that the sensing element would assume. The other two arms were fixed resistors of equal value. After calibration, any temperature could be selected by adjusting the variable resistor to the resistance value that the sensing element would assume at the desired temperature. The unbalance of the bridge was amplified and used to operate a relay system which supplied current to the heater in an on-off or a maximum-minimum type of variation. When a stable temperature was established, the bridge oscillated about a balance point with current being pulsed to the heater. This oscillation was so small, however, that

it was possible to limit sample temperature variation to

± 0.05°K or better over the entire temperature range.

Sample temperatures were measured by the thermometer,
consisting of a thermocouple, a carbon resistor, and a coil
of tantalum wire, shown in Figure 2, which was located below
the sample position in the sample chamber. It was impossible
to mount the thermometer on the sample holder since this
would lower the precision of the analytical balance. A
copper-constantan thermocouple served as the primary thermom-
eter from 4.2°K to 300°K. It was tested initially at helium
and nitrogen bath temperatures, and the differences in emf
from the values of a much more extensively calibrated
thermocouple taken from the same spools of wire were used to
establish a calibration. The 4.2°K calibration check point
was redetermined during each helium liquid run and suitable
corrections were made. A length of tantalum wire wound on
the carbon resistor served as a fixed temperature point at
low temperatures. Its superconducting transition temperature
was independently determined to be 4.38°K. Temperatures from
1.3°K to 20°K could be measured with the previously calibrated
carbon resistor which could also be checked during each run
at 4.38°K. An additional measure of temperatures below 4.2°K
could be made by assuming that the sample and the liquid bath
were at the same temperature. Liquid bath temperatures were
determined by measuring the pressure above the bath with

manometers mentioned previously and converting these pressure values to corresponding temperatures. The temperature difference between sample and bath at 4.2°K was determined to be less than 0.02°K.

A determination of the correspondence of sample temperature to thermometer temperature was made. A small coil of tantalum wire and a thermocouple were fastened in the sample holder at the sample position. The temperature was adjusted until the tantalum coil on the thermometer was just superconducting. The temperature was then increased until the tantalum coil in the sample holder went superconducting. The temperature difference was measured by the carbon resistance thermometer. The difference was less than 0.02°K. The thermocouple, which had been calibrated against a platinum resistance thermometer at liquid nitrogen temperature, was used to check the temperature difference at 76°K. The difference between the two thermocouples was within the error of calibration. Sample temperatures are therefore believed correct to one-half degree above 4.2°K and to about 0.1°K below 4.2°K.

It has been established that it is not possible to design a field configuration which will give both weighing stability and horizontal stability simultaneously. A sample centering method described by Thoburn (59) and described as a "wiggler" was modified as shown in Figure 2. Silk threads were used to

transmit power to the wiggler from outside the dewar. The upper end of one thread was fastened to the rim of a variable speed disc so that rotary motion could be changed to translatory motion. The upper end of the other thread was fastened to a tension spring which provided the necessary restoring force.

Single crystal samples tend to turn so as to align certain preferred directions along any applied magnetic field. In order to make measurements with the field applied along the c-axis for temperatures below 50°K, it was found necessary to use a set of four centering chains fastened to flat vanes in the upper end of the rigid quartz rod supporting the sample holder. This system has been described by behrendt (56). With this system, the balance was not so sensitive as before, but measurements of weight could be made to within one per cent.

C. Method and Apparatus for Electrical
Resistivity Measurements

Electrical resistivity measurements from 4.2°K to 300°K were also made on the three holmium single crystals. The resistance of each sample was determined by measuring the potential drop across the sample and the current passing through the sample. The current, I, was measured by measuring the potential drop across a standard resistance placed in series with the sample. The effects of thermal emfs produced

by local heating at points of contact resistance were
cancelled by measuring the potential drops with the current
passing through the sample in first one direction and then
in the opposite direction. The average of the two values, V,
was used in further calculations.

Resistivity values were determined by use of the
equation

$$\rho = \frac{V}{I}\frac{A}{l} \tag{4.4}$$

where A is the cross-sectional area and l is the distance
between potential probes, or effective length of the sample.

The dimensions of the samples were measured with a
traveling microscope. Determinations of width were made at
three approximately equidistant positions on each face of the
samples. Six measurements were made at each position. The
effective length of the sample was determined by measuring
the distance between the narrow impressions left by the
razor-blade edges of the potential contacts.

The residual resistivity for each sample was determined
by extrapolation of the low temperature resistivity values to
zero degrees Kelvin. The value obtained was then subtracted
from the experimentally determined resistivity, and the result
was plotted as a function of temperature.

Electrical resistivity measurements were made in a
cryostat described by Colvin, et al. (6). Temperatures were
measured with a copper-constantan thermocouple and controlled

by the automatic temperature controller described in the
section on magnetic measurements. The thermocouple was
calibrated at the beginning of each series of measurements
at liquid helium temperatures. With no power being supplied
to the sample or the heat leak chamber, and with helium
exchange gas at several millimeters of mercury pressure
giving good thermal contact with the liquid helium, the
reading of the thermocouple at temperature equilibrium was
ascertained, and this was assumed to be its value at 4.2°K.
Temperatures were considered accurate to one-half degree.

Liquid helium was used to obtain temperatures from 4.2°K
to 100°K. Liquid nitrogen was used to cover the temperature
range from 80°K to 300°K.

A modified four-probe sample holder shown in Figure 3
was constructed for making resistivity measurements on the
samples previously used in magnetic measurements. The
potential probes (P) consisted of small bits of razor blades
approximately 2 mm square soldered to brass screws which were
mounted in a red fiber positioning strip. The sharp edges
of the razor blades gave extremely narrow contact lines for
the potential measurement. Phosphor bronze spring contacts
(C) were used for current probes at the ends of the sample.
The thermocouple (T.C.) was positioned in the sample holder
so that it was separated from the sample by only a thin piece
of tissue paper. A copper band (b) held the potential probes
in contact with the sample.

Figure 3. Sample holder for the electrical resistivity measurements.

B. Band which held potential contacts to sample

C. Current contacts

P. Potential contacts

T.C. Copper-constantan thermocouple

TRANSVERSE CROSS
SECTION

LONGITUDINAL CROSS
SECTION
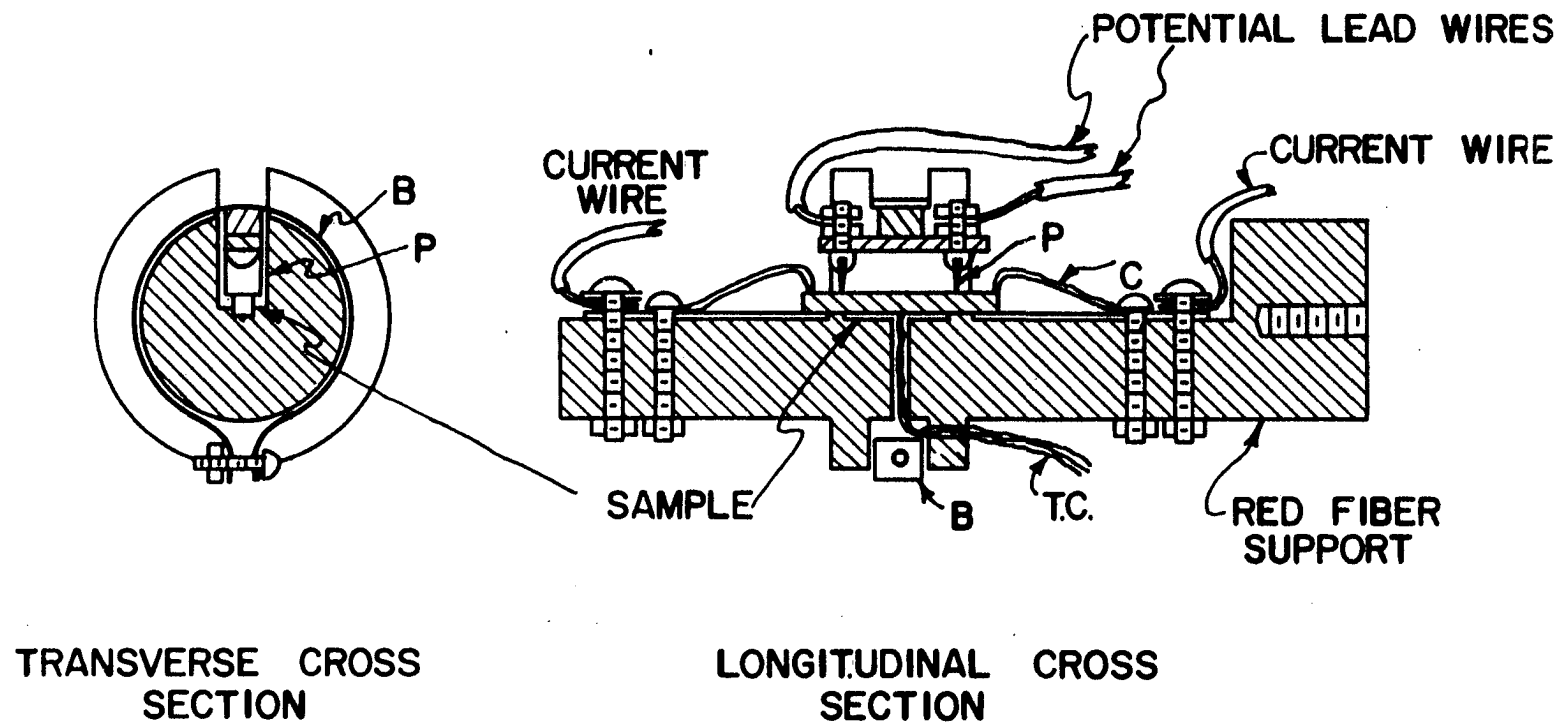
V. RESULTS

### A. Magnetic Measurements; a-axis Crystal

Isothermal measurements of the magnetic moment per gram, σ, of the a-axis crystal were made as a function of magnetic field at temperatures from 1.8°K to 296.8°K. All measurements above 77°K were taken with the basal plane of the sample placed in a horizontal position. After these higher temperature measurements were completed, the low temperature measurements were begun. It was observed, however, that for an isotherm of 4.2°K and at magnetic fields above 12,000 oersteds, the crystal turned so that the $\langle 10\bar{1}0 \rangle$ direction was aligned with the field. The crystal was then reoriented in the sample holder so that the basal plane was vertical and the a- and c-axes were in a horizontal plane. All measurements below 77°K were made with this crystal orientation except for a measurement at 30°K which will be discussed later.

The data are presented as isotherms in Figures 4, 5, 6, and 7. Isofield curves where the magnetic moment per gram is plotted versus temperature for several constant magnetic fields were obtained from these isotherm curves and are given in Figures 8 and 9. Figure 9 shows the detail of a Néel point which is seen to be field dependent. Its value extrapolated to zero magnetic field is 132°K.

The anomalous behavior of the magnetic moment in the

Figure 4. Isotherms for the a-axis crystal from 127.4°K to room temperature. The 127.4°K and 130.4°K isotherms show the effect of the magnetic field upon the Néel point.

HO a-AXIS CRYSTAL

$\sigma_{H,T}$

H (KILO-OERSTEDS)

127.4°
130.4°
135.5°
140.1°
151.2°
181.1°
214.1°
251.2°
296.8°

44
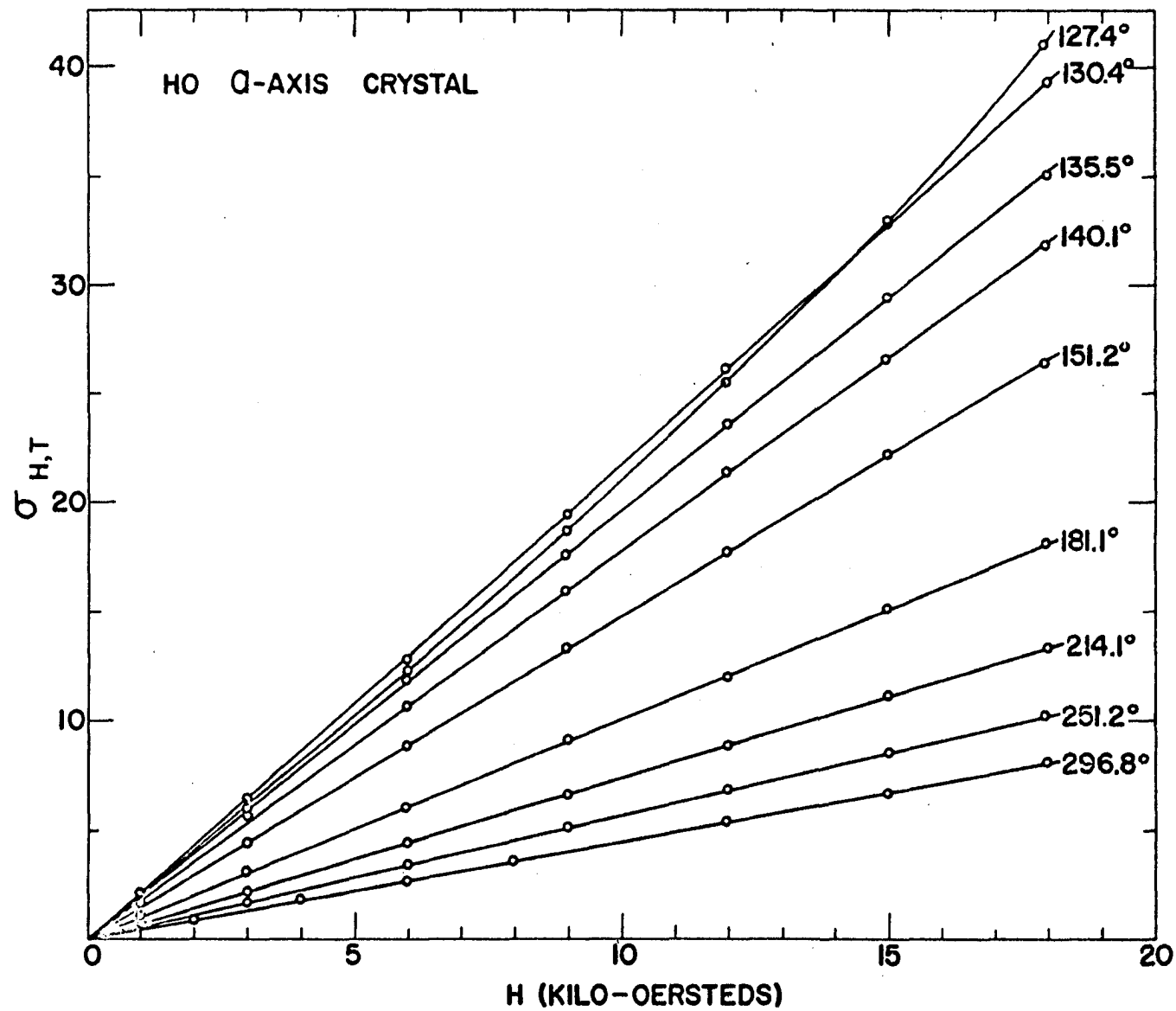
Figure 5. Isotherms for the a-axis crystal in the antiferromagnetic region near the Néel point.
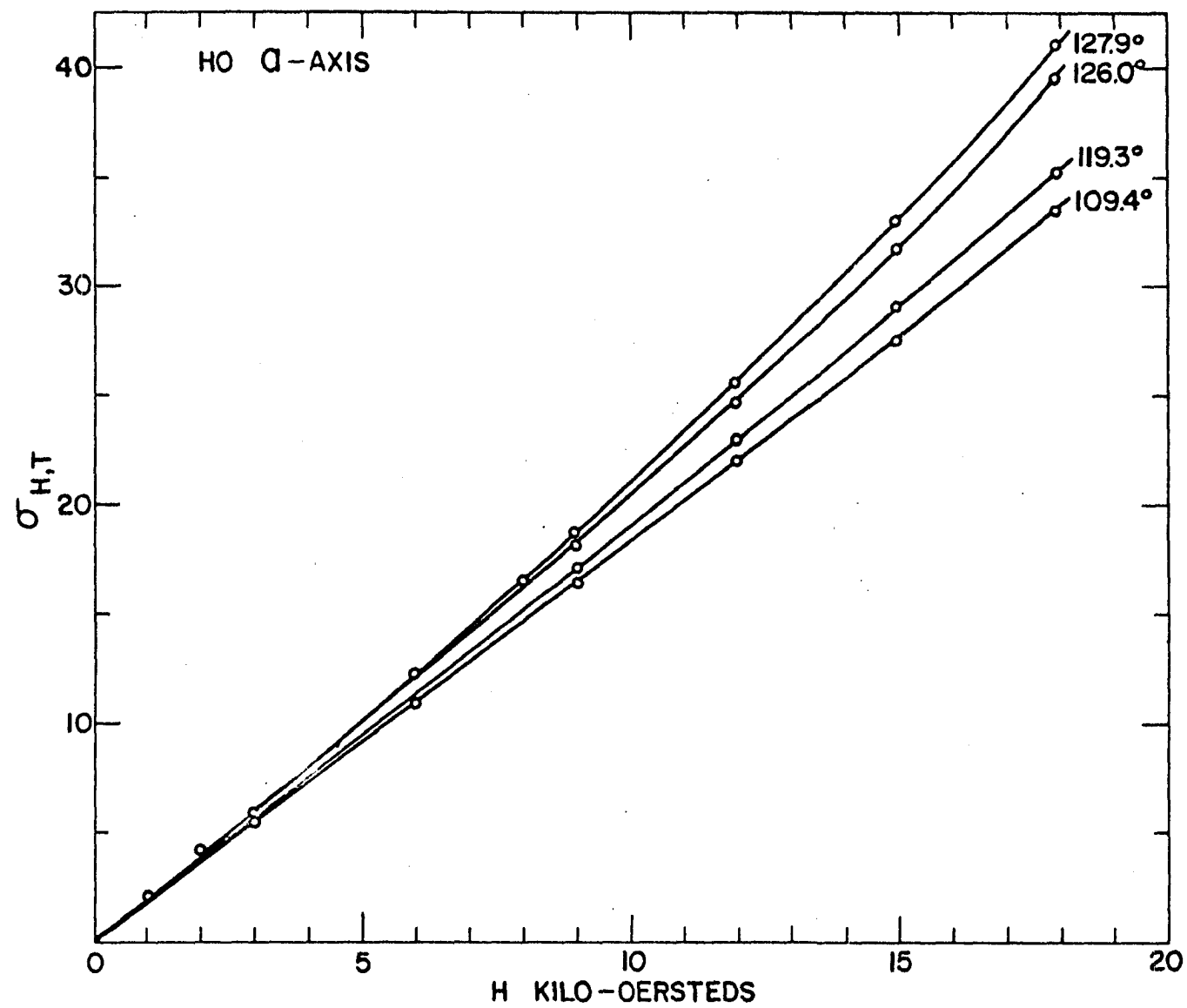
Figure 6. An expanded plot of the low moment portions of isotherms for the a-axis crystal below 109.4°K.

HO a-AXIS CRYSTAL

$\sigma_{H,T}$

H (KILO-OERSTEDS)

9.0° 22.2° 24.6° 30.0° 35.0° 40.4° 45.0° 50.0° 61.8° 74.0° 79.2° 88.9° 99.7°
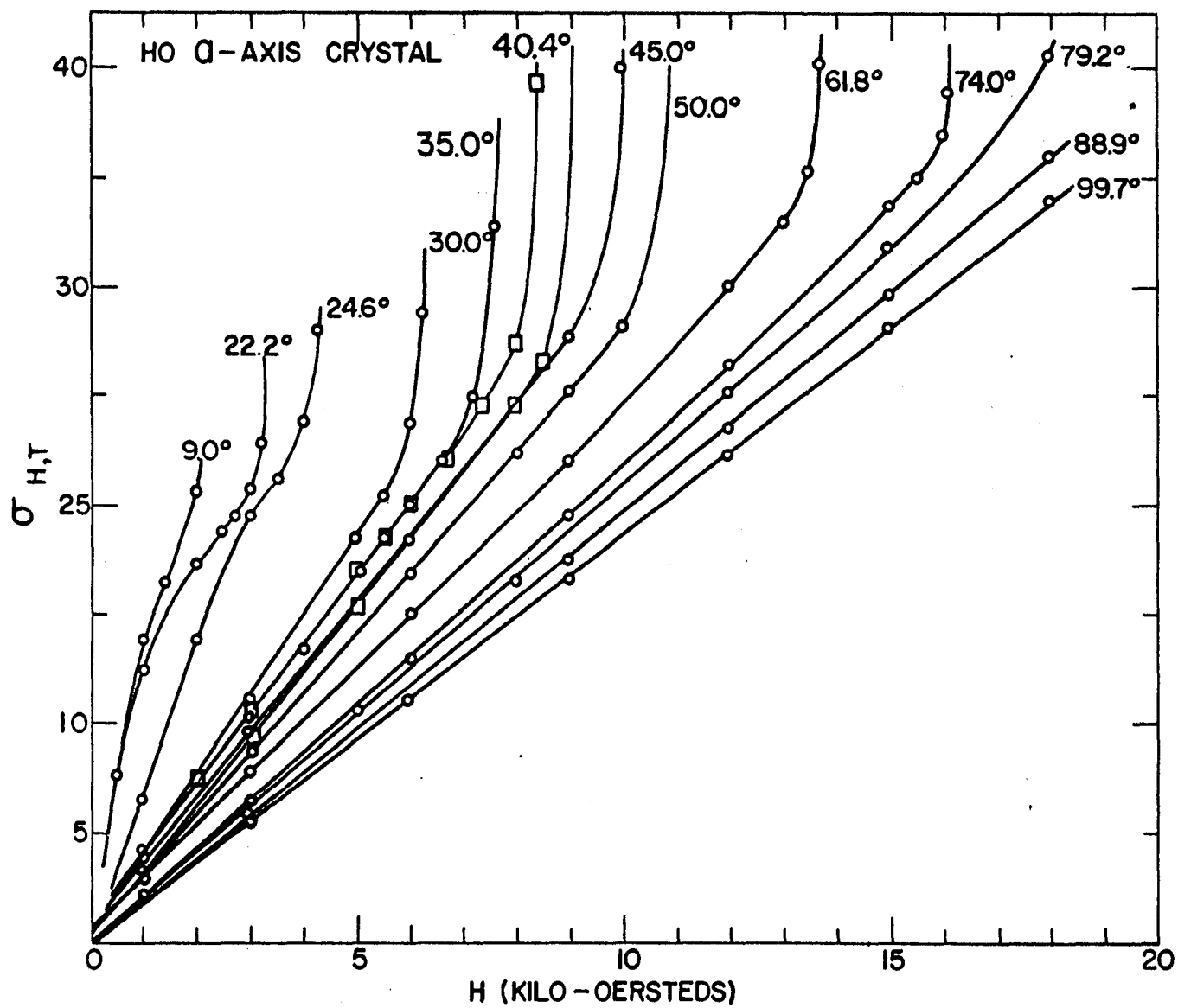
Figure 7. Isotherms for the a-axis crystal in the antiferromagnetic and ferromagnetic regions. Dashed lines and square data points show isotherms taken with decreasing fields.

HO α – AXIS CRYSTAL

$\sigma_{H,T}$

H (KILO-OERSTEDS)

50
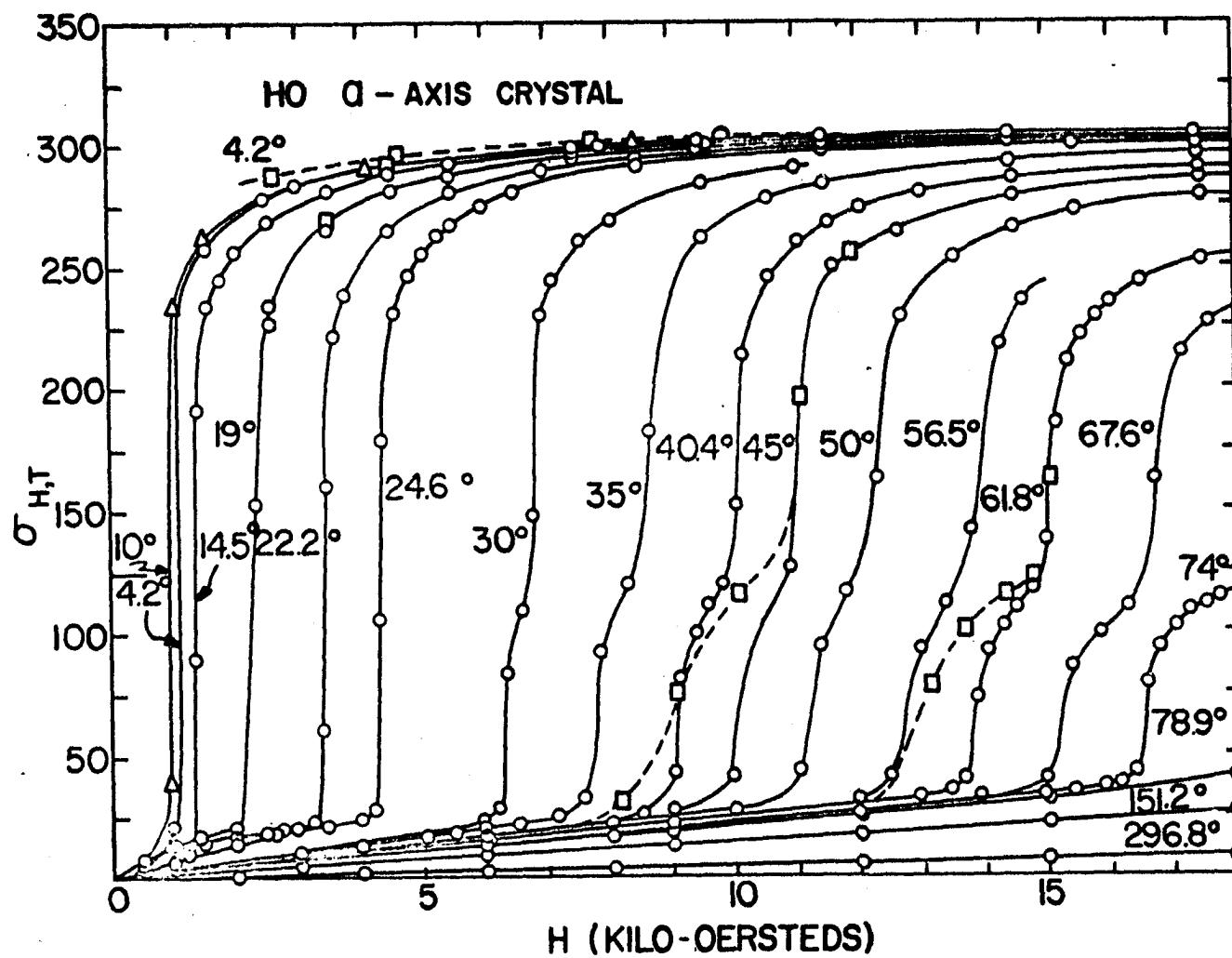
Figure 8. Isofield curves for the a-axis crystal. The inset shows the small
          peak which occurred at 20°K.
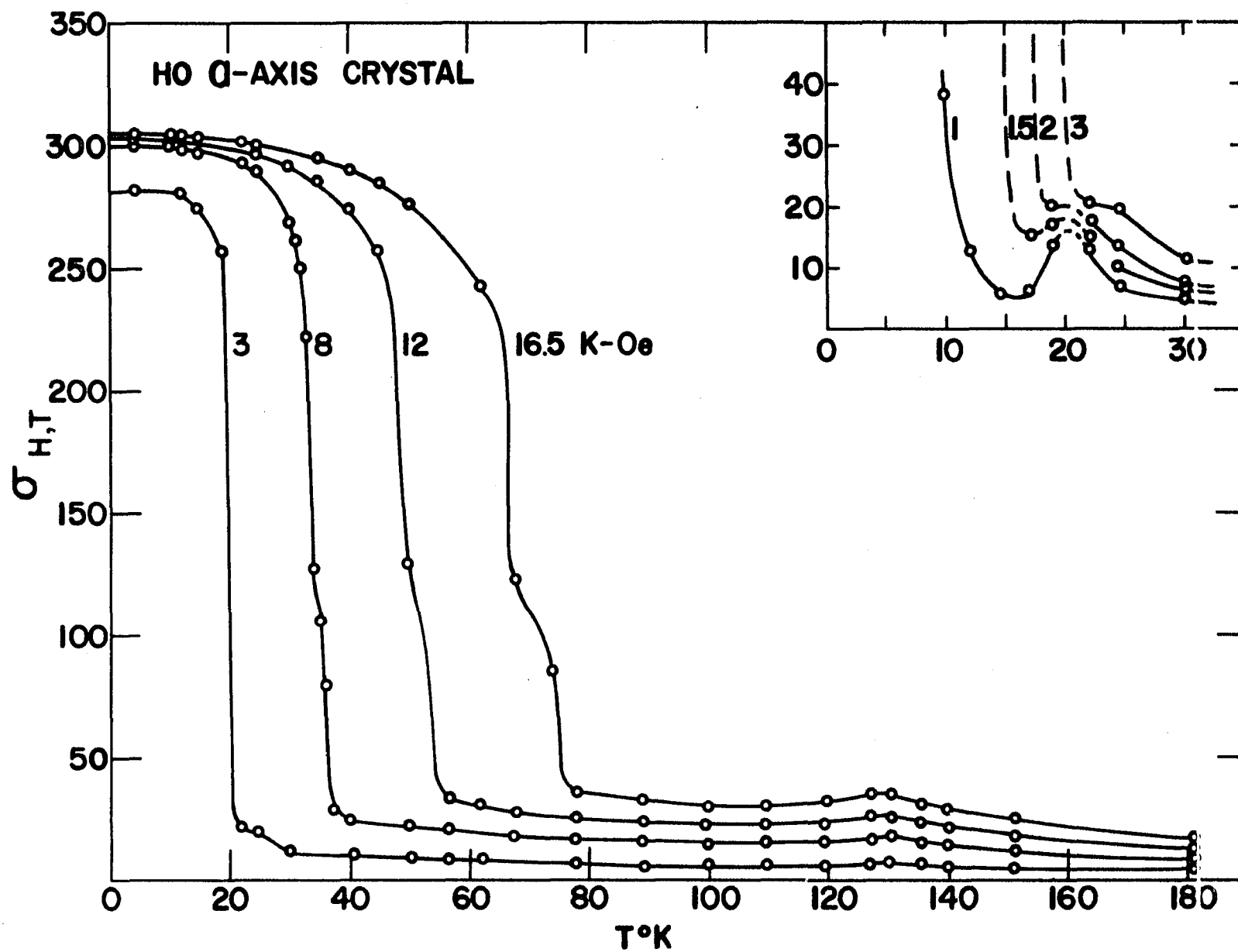
Figure 9.   An expanded plot of the isofield curves for the a-axis crystal in
the neighborhood of the Néel point.
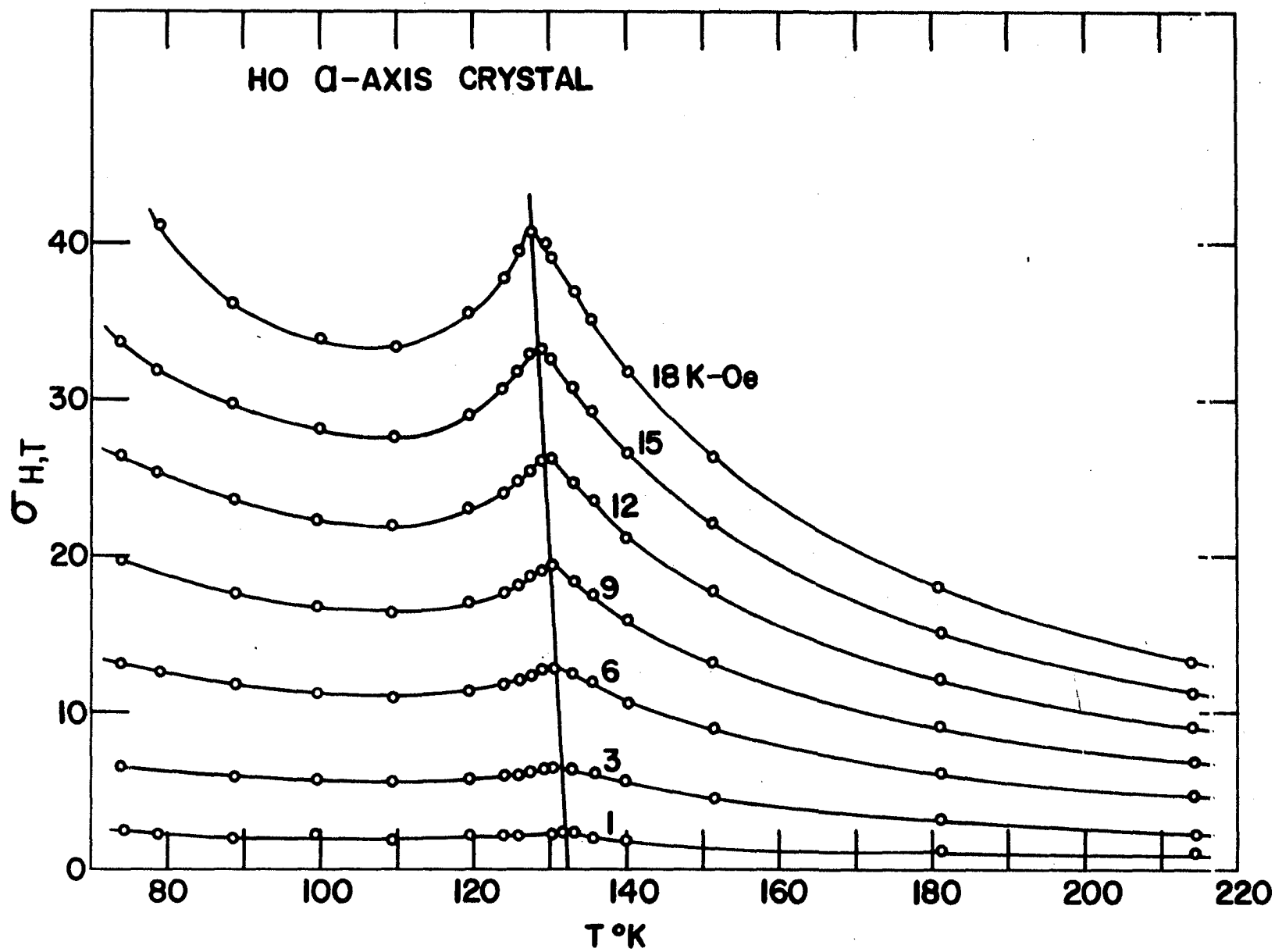
antiferromagnetic temperature range is shown in Figure 7.
The "knee" which appears at a magnetic moment of about 100
cgs units per gram for all isotherms above 30°K was not
observed in the measurements of Green, et al. (12) and
Behrendt, et al. (10) for single crystals of erbium and
dysprosium. They observed only an almost discontinuous rise
followed by rapid saturation of the magnetic moment.

The "knee" also appears in the isofield plot of Figure
8. The circles indicate points taken from experimental
isotherms. The details of the curves in the regions of the
knees were established by drawing extra isotherms at one
degree temperature intervals between those actually measured,
using the experimental curves as guides. Although some error
is inherent in this procedure, the result is a more realistic
representation of the magnetic behavior than would be given
by smooth curves drawn through the experimentally determined
points.

Measurements of magnetic moment as a function of
decreasing fields were made at several temperatures to check
for the hysteresis reported by Rhodes, et al. (9) for poly-
crystalline holmium. Curves for decreasing fields are
indicated by dashed lines in Figure 7. The uncertainty of
calibration of the magnet for decreasing fields results in
an error estimation of about two per cent in the value of
magnetic moment and 0.2 kilo-oersted in the value of the

magnetic field. The hysteresis in the antiferromagnetic range, as shown at 45°K and 61.8°K, occurs at the "knee" described previously. The decreasing curve runs parallel to the increasing curve below this knee and merges with the linear portion of the increasing curve at a lower value of applied field. The width of the hysteresis loop thus formed is approximately the same as the width of the "knee" on the increasing curve.

When an attempt was made to make measurements at the 30°K isotherm, the sample turned so that the c-axis was aligned with the magnetic field. No such effect was observed at 24.6°K or at 35°K. The sample was then removed from the sample holder and reoriented so that the c-axis was vertical and the basal plane was horizontal. The sample turned through an angle of 15° or so when measurements were made in the region of the "knee" of the curve, but at points above the "knee" the sample once again lined up with the magnetic field. Then at fields above twelve kilo-oersteds the sample turned through an angle of 30° to align the $\langle 10\bar{1}0 \rangle$ direction with the magnetic field.

A small peak in the magnetic moment versus temperature isofield curve which occurs at 20°K for small magnetic fields is shown in the inset of Figure 8. The peak is not present for magnetic fields greater than three kilo-oersteds.

A determination of the saturation moment for the a-axis

crystal, $\sigma_{\infty,0}$, at 0°K and infinite magnetic field is shown
in Figure 10. The high magnetic field values of $\sigma_{H,T}$ were
plotted versus $\frac{1}{H^2}$ for several low temperatures. The resulting
straight lines were extrapolated to $\frac{1}{H^2} = 0$ to obtain values
of $\sigma_{\infty,T}$. In Figure 11 values of $\sigma_{\infty,T}$ are shown plotted
versus $T^{3/2}$ and also T^2. An extrapolation to $T = 0$ gives
values of $\sigma_{\infty,0}$. There is little choice between the $\sigma_{\infty,T}$
versus $T^{3/2}$ plot and the $\sigma_{\infty,T}$ versus T^2 plot.

A determination of the spontaneous magnetization, $\sigma_{0,0}$,
is also shown in Figure 11. An excellent discussion of
various methods of determining spontaneous magnetization has
been given by Arajs and Miller (64). Values of $\sigma_{0,T}$ for the
holmium data were determined by extending the high field,
linear portion of the isothermal magnetization curves to zero
field where the intersections with the ordinate gave $\sigma_{0,T}$.

A plot of $\frac{1}{X}$ versus T for the a-axis crystal paramagnetic
data is shown in Figure 12.

B. Magnetic Measurements; $\langle 10\bar{1}0 \rangle$ Crystal

Isothermal measurements of the magnetic moment per gram
of the $\langle 10\bar{1}0 \rangle$ crystal were made as a function of magnetic
field at temperatures from 1.4°K to 296.8°K. All measure-
ments were taken with the basal plane of the crystal placed
in a vertical position so that the $\langle 10\bar{1}0 \rangle$ direction and the
c-axis were in a horizontal plane. No turning of the sample
was observed at any temperature.

Figure 10. Isothermal variation of the magnetic moment as $\underline{a}$ function of $1/H^2$ for the a-axis and the $<10\overline{1}0>$ crystals.
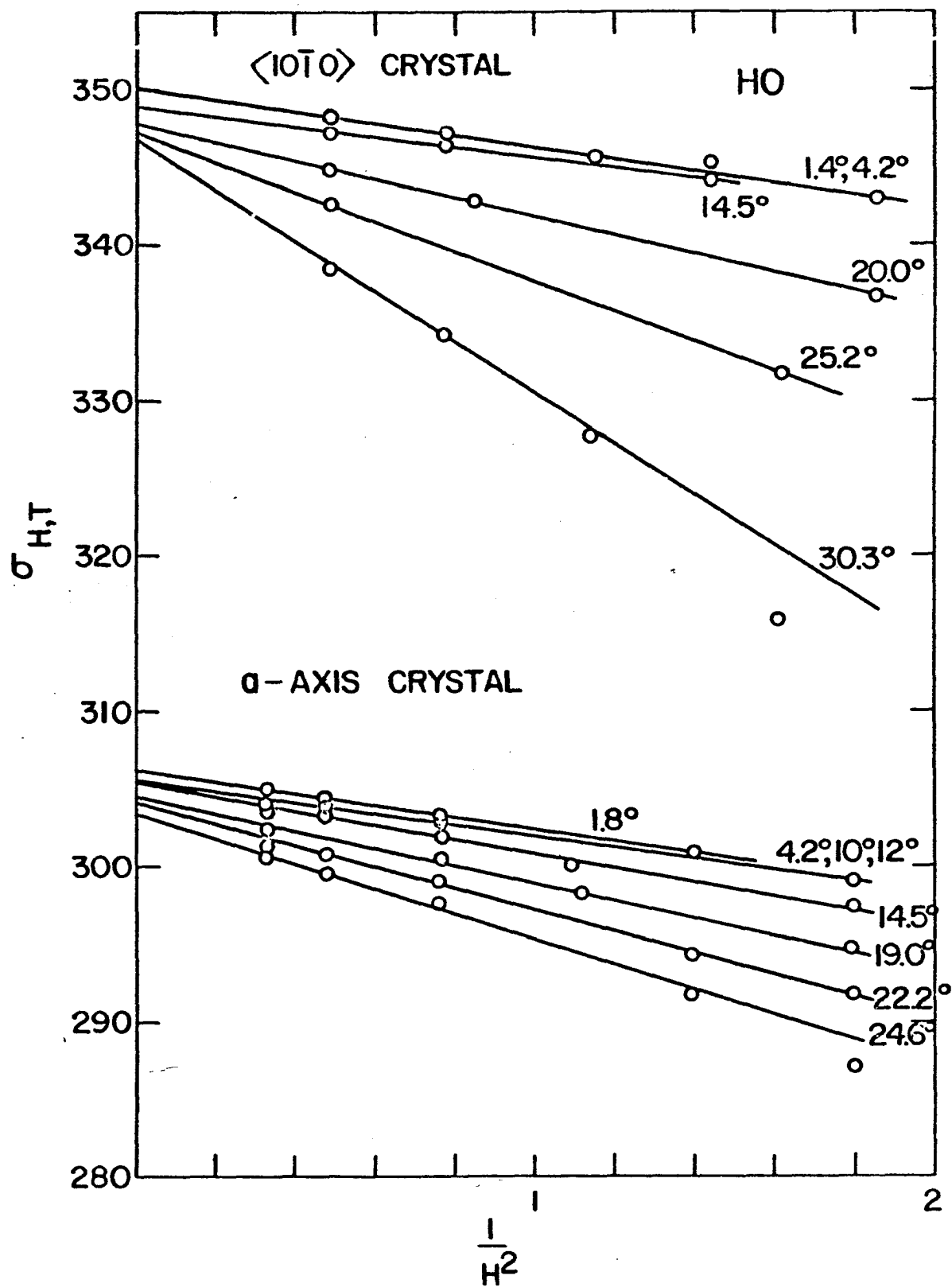
Figure 11. Saturation and spontaneous magnetization of
            the $<10\bar{1}0>$ and the a-axis crystals as a function
   of $T^{3/2}$ and T^2.
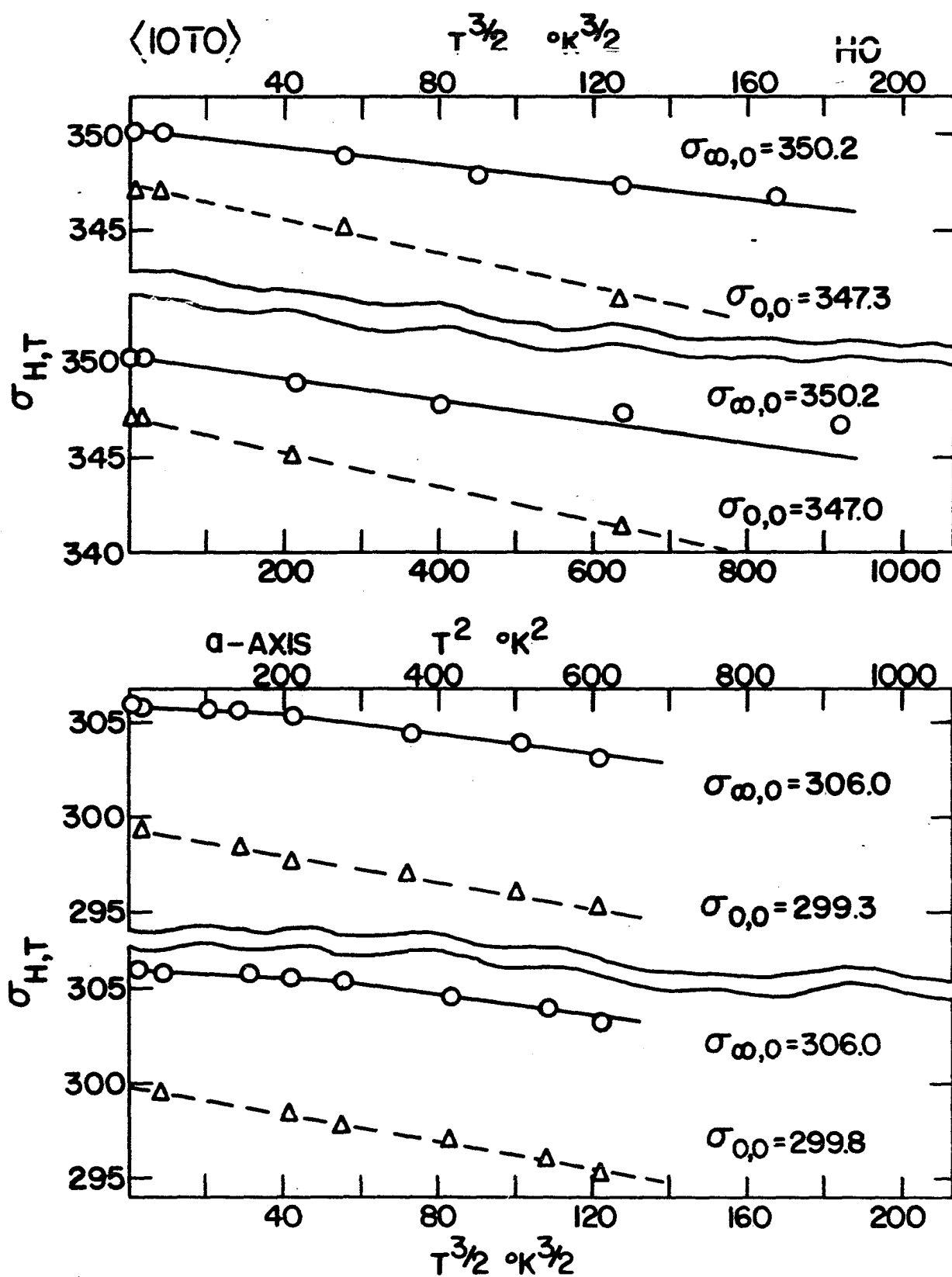
Figure 12. Plots of 1/X as a function of temperature for the a- and c-axis
crystals and for a polycrystalline sample of holmium.
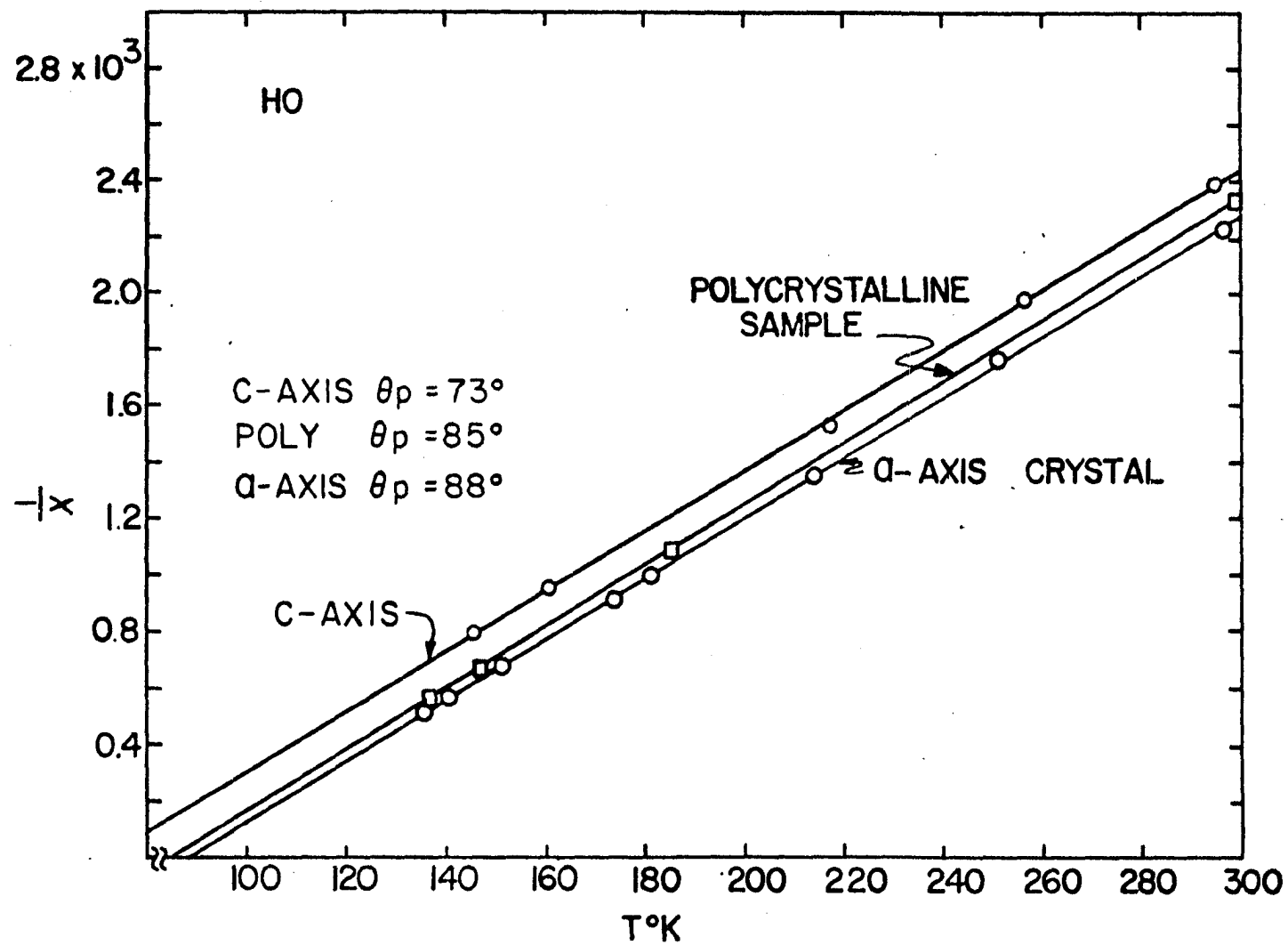
The data are presented as isotherms in Figures 13 and 14.
Isofield curves obtained from the isotherm data are given in
Figure 15. The data for the a-axis crystal and the $\langle 10\bar{1}0 \rangle$
crystal coincide above 80°K, so that the Néel point data of
Figure 9 and the $\frac{1}{X}$ versus T data of Figure 12 for the a-axis
crystal are also representative of the $\langle 10\bar{1}0 \rangle$ crystal
behavior. At lower temperatures, the data for the two crystals
do not coincide. Anisotropy exists in the basal plane, and
the $\langle 10\bar{1}0 \rangle$ direction is the direction of easy magnetization.

An anomalous behavior more complicated than that of the
a-axis crystal is exhibited in Figure 14 by the $\langle 10\bar{1}0 \rangle$ crystal
in the antiferromagnetic temperature range. Two "knees"
appear in the isotherm data above 45°K. The first "knee"
appears at a magnetic moment of approximately 100 cgs units
per gram, and the second "knee" appears at approximately 200
cgs units per gram. The widths of the "knees" increase with
increasing temperature, but the values of magnetic moment at
which they appear seem to be constant. The details of the
isofield curves for Figure 15 have been determined in the
manner described in Chapter V, Section A for the a-axis
crystal in order that the effect of the "knees" could be
properly described.

The dashed lines in Figure 14 show the results of
measurements of magnetic moment taken at decreasing fields
to determine the presence of magnetic hysteresis.

Figure 13.   Isotherms for the <10$\bar{1}$0> crystal in the paramagnetic region plus the low moment portions of isotherms in the antiferromagnetic region.

HO <10$\bar{1}$0> CRYSTAL

$\sigma_{H,T}$

H (KILO-OERSTEDS)

130.0°
120.0°
91.2°
110.3°
140.3°
160.8°
188.6°
219.1°
246.1°
296.3°

30.3°
40.3°
49.6°
60.8°
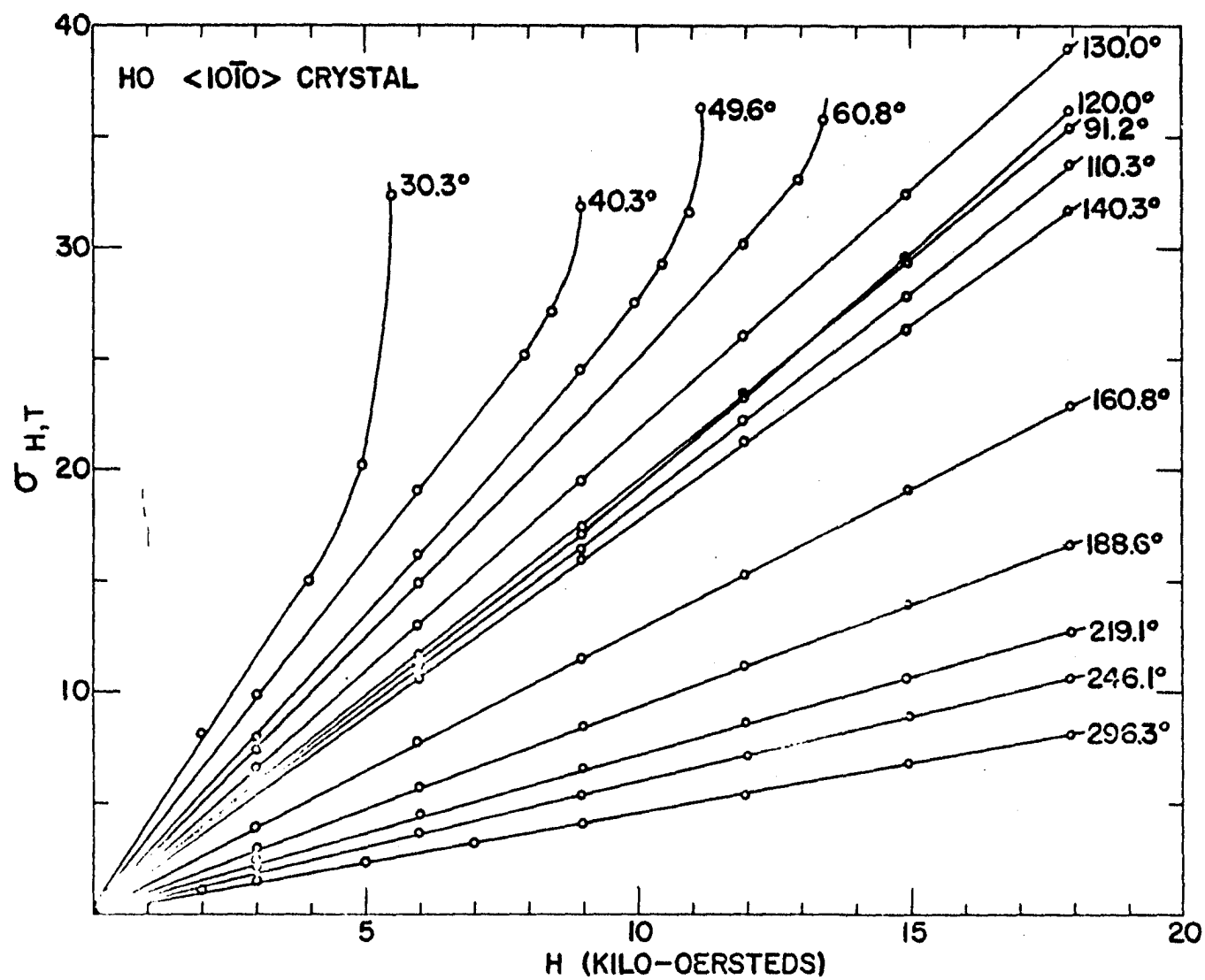
Figure 14. Isotherms for the <10$\overline{1}$0> crystal at low temperatures. The dashed
lines and the square data points show isotherms taken at decreasing
magnetic fields.
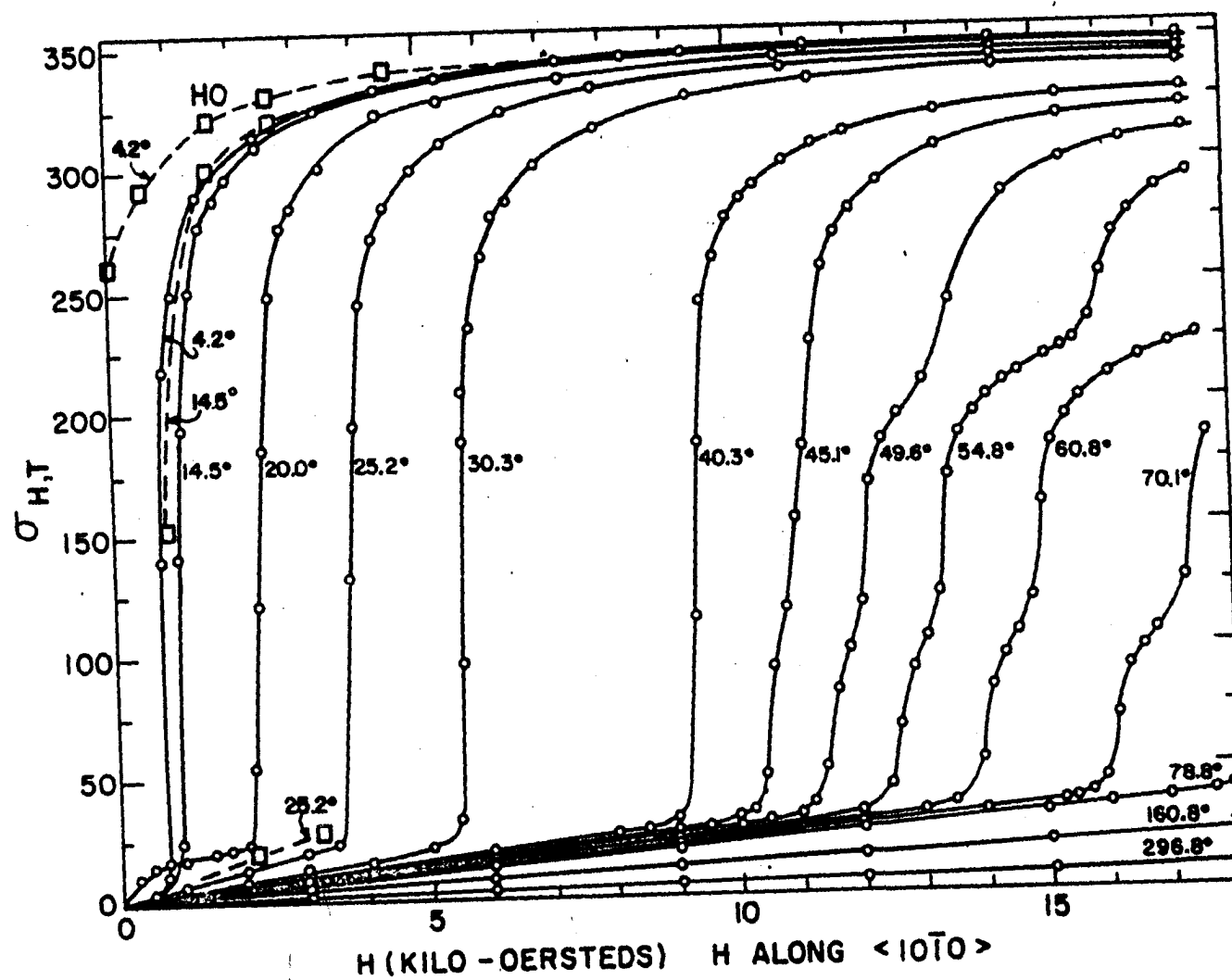
Figure 15. Isofield curves for the <10$\bar{1}$0> crystal.

HO <10$\bar{1}$0> CRYSTAL

$\sigma_{H,T}$

3   8 11 13   16 K-Oe

T°K
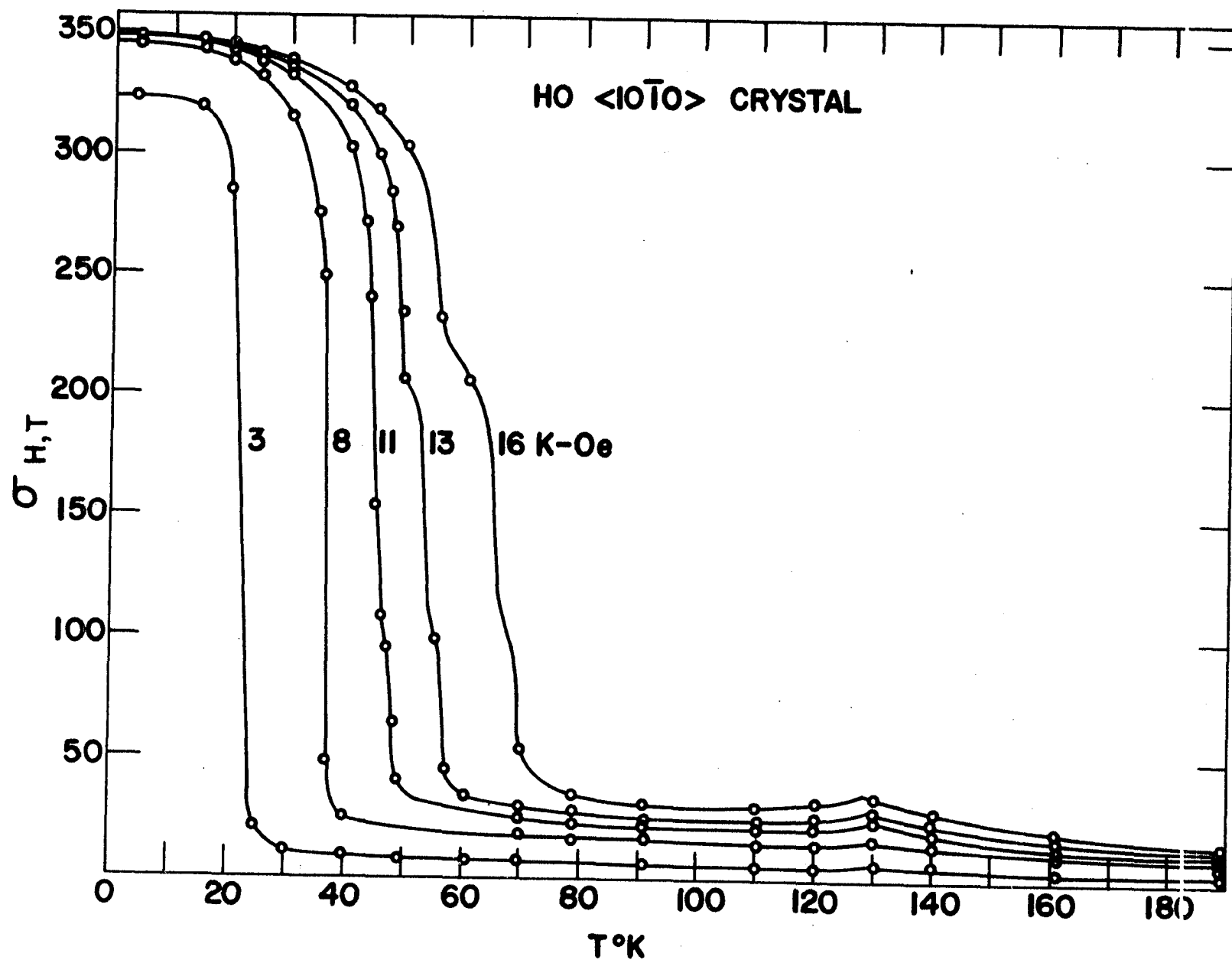
Values of the saturation moment, $\sigma_{\infty,0}$, and the spontaneous magnetization, $\sigma_{0,0}$, for the $\langle 10\bar{1}0 \rangle$ crystal were determined in the manner described in Chapter V, Section A.

C. Magnetic Measurements; c-axis Crystal

The magnetic moment per gram of the c-axis crystal was measured isothermally as a function of magnetic field at temperatures from 1.4°K to 295.6°K. Measurements at temperatures below 50°K were made using the system of chains described in Chapter IV, Section A to keep the c-axis parallel to the direction of the magnetic field.

The isotherm data are presented in Figures 16, 17, and 18, and the isofield curves obtained from the isotherm curves are shown in Figure 19. Decreasing field data are shown by dashed lines. Experimental points are indicated by squares. Also plotted in Figure 18 is the 4.2°K isotherm for the $\langle 10\bar{1}0 \rangle$ crystal so that it can be compared to the 4.2°K isotherm of the c-axis crystal.

The isotherms below 20°K in Figure 18 show an initial magnetization of about 60 cgs units per gram. The scatter of the data at fields below one kilo-oersted may be attributed to the lack of a good magnet calibration in this range. The small positive slopes of the curves up to 18 kilo-oersteds indicate that holmium is very hard magnetically in the direction of the c-axis.

The isofield curves of Figure 19 do not show the Néel

Figure 16. Isotherms for the c-axis crystal in the paramagnetic region and
the upper portion of the antiferromagnetic region.
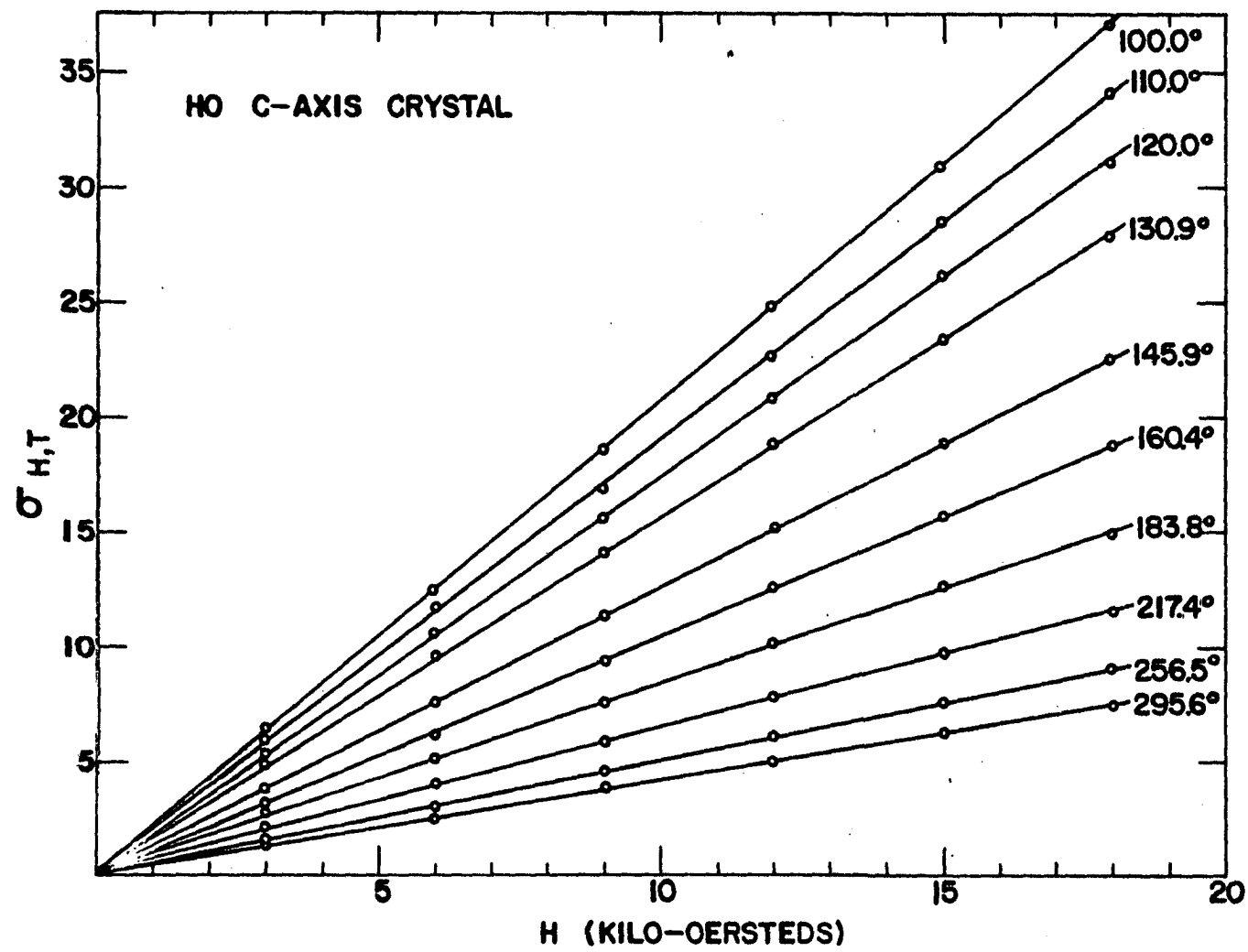
Figure 17. Isotherms for the c-axis crystal at intermediate temperatures in the antiferromagnetic region.
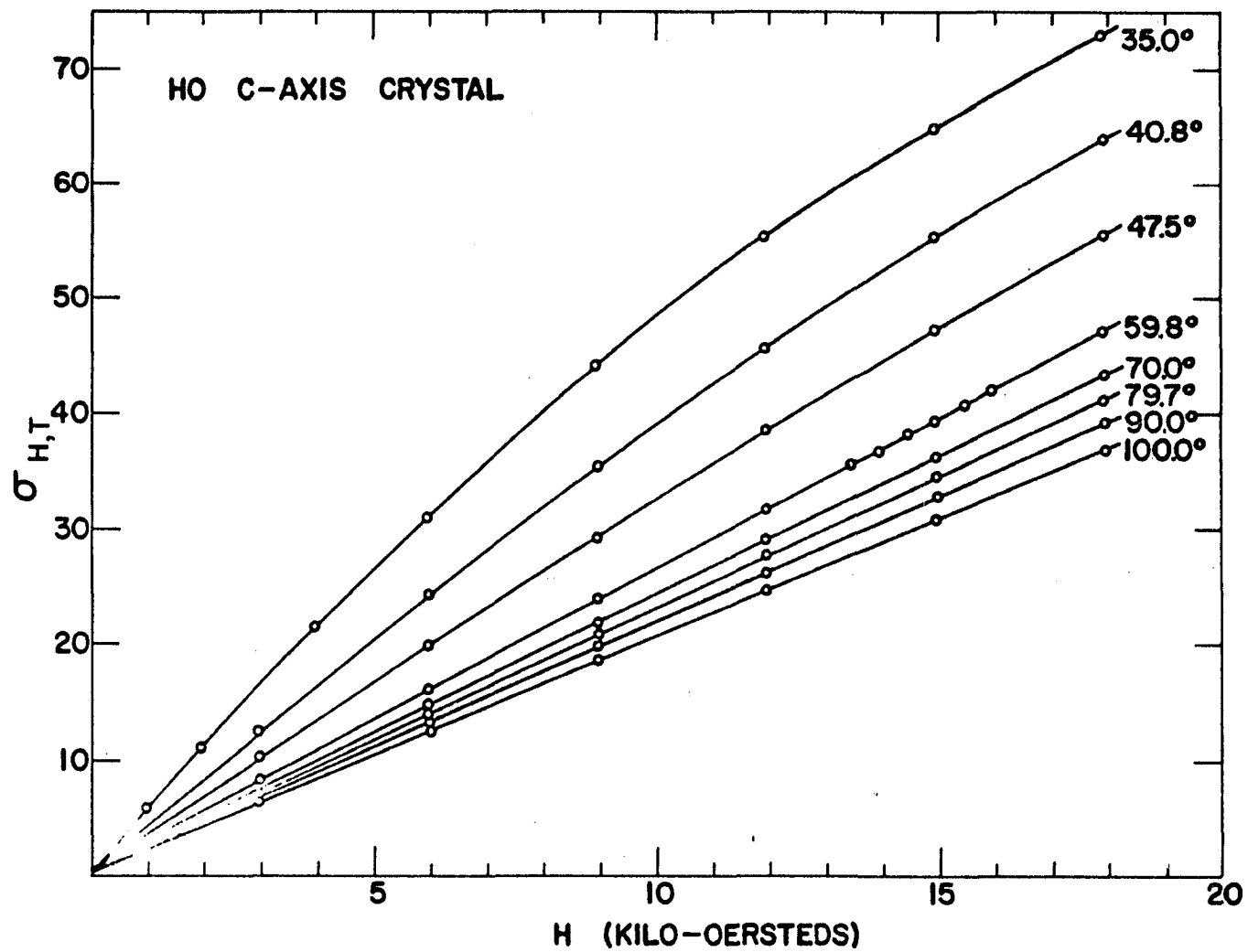
Figure 18. Isotherms for the c-axis crystal. Dashed lines and square data
points indicate measurements taken with decreasing fields. A
4.2°K isotherm of the <10$\bar{1}$0> crystal is given for comparison.
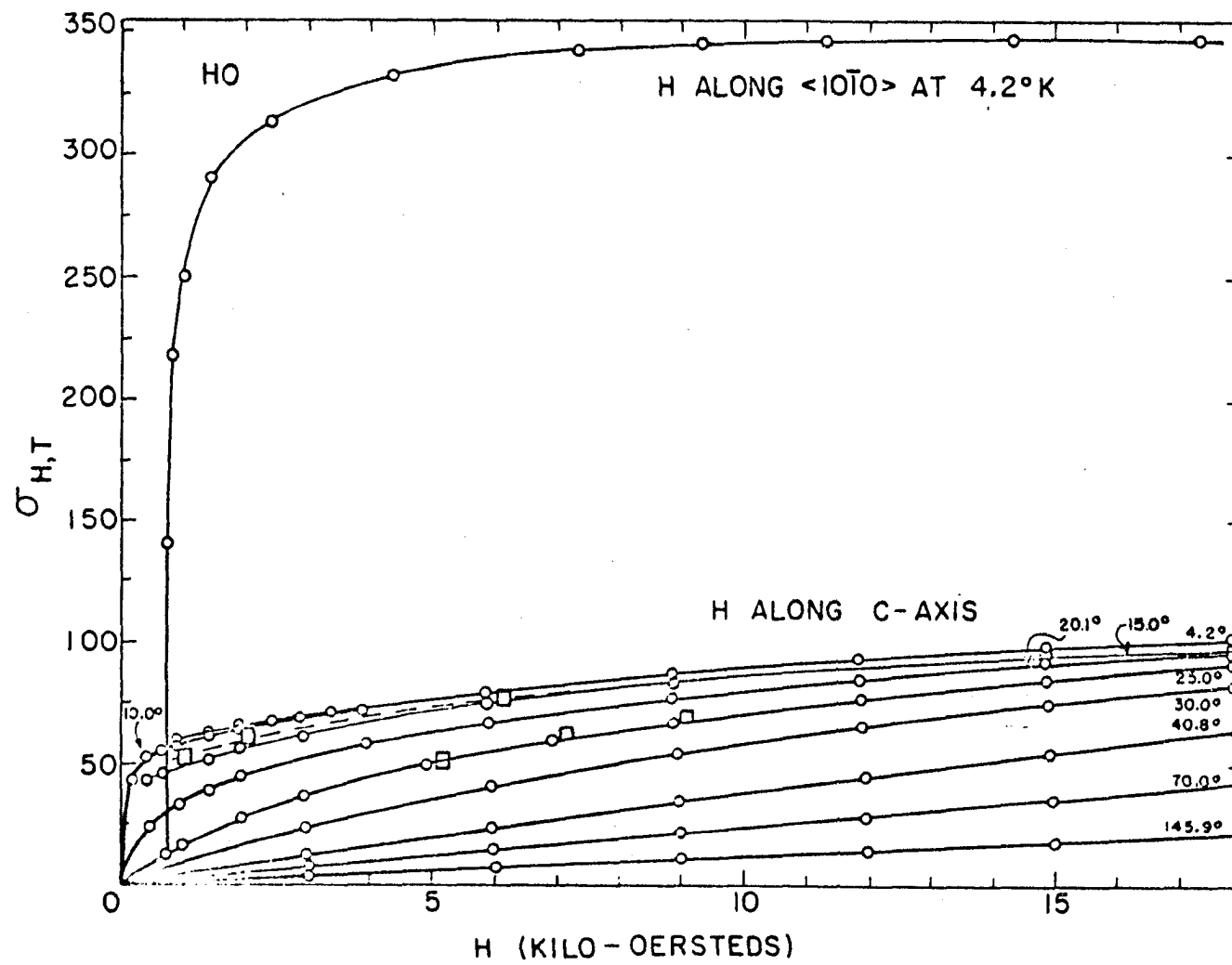
Figure 19.   Isofield curves for the c-axis crystal.

HO C-AXIS CRYSTAL

18 K-Oe
15
12
9
6
3

$\sigma_{H,T}$

T °K
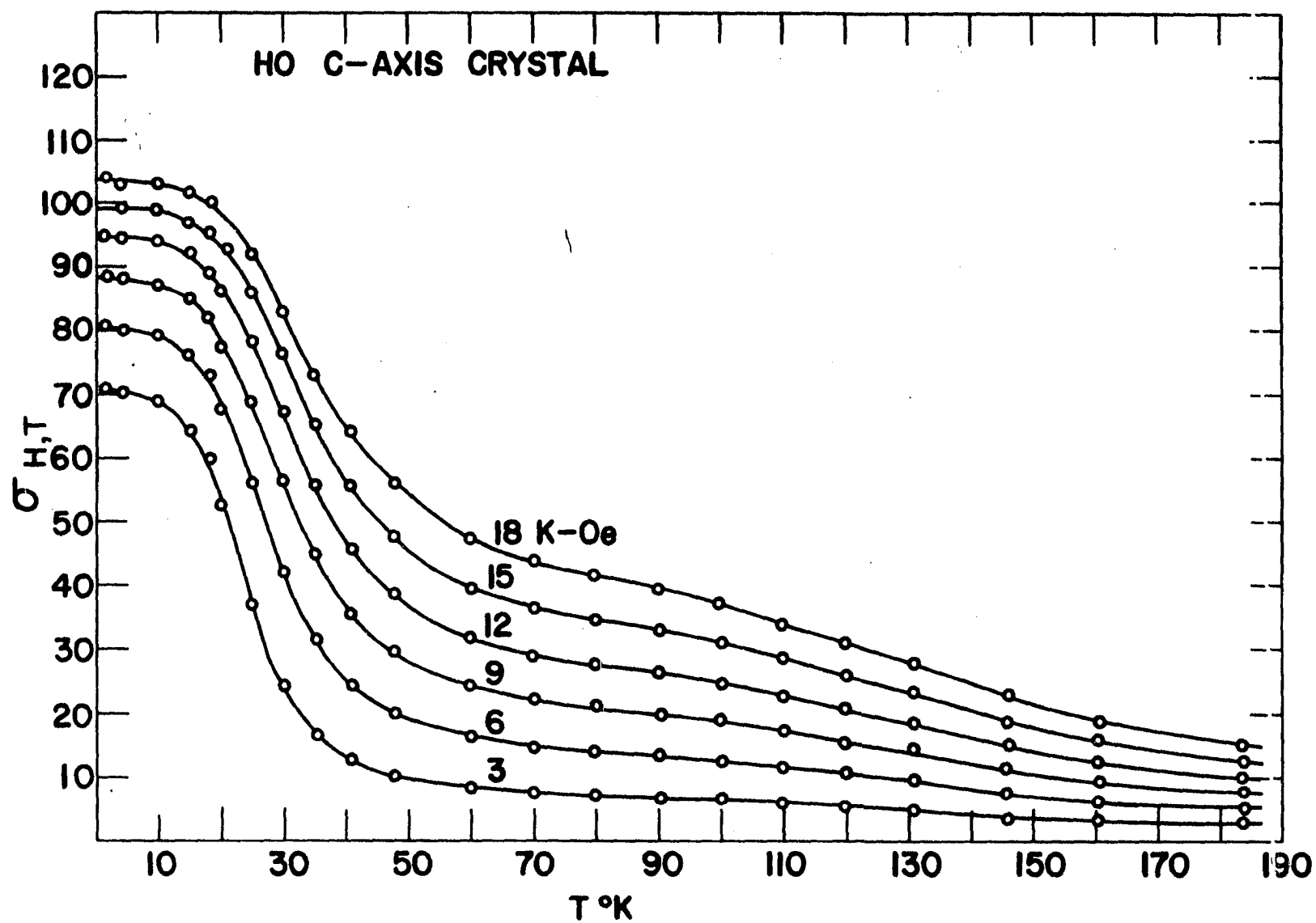
point at 132°K which was observed for the a-axis and $\langle 10\bar{1}0 \rangle$ crystals.

In Figure 12 the $\frac{1}{X}$ versus T plot for the c-axis crystal paramagnetic data are shown. Also shown are the experimental data points for polycrystalline holmium reported by Rhodes, et al. (9). Calculated values of magnetic susceptibility for a polycrystalline sample, X_{poly}, were obtained from single crystal results by use of the relationship

$$X_{poly} = \frac{2\ Xa + Xc}{3} \tag{5.1}$$

where X_a is the susceptibility of the a-axis crystal and X_c is the susceptibility of the c-axis crystal. The straight line between the a-axis and c-axis lines is a plot of $\frac{1}{X_{poly}}$ versus T. The data of Rhodes fall quite close to this line although their slope is slightly different.

D. Resistivity Measurements

The electrical resistivities (minus residual) of the a- and c-axis crystals are displayed in Figure 20 as functions of temperature. Since the data for the a-axis and the $\langle 10\bar{1}0 \rangle$ crystals coincided within experimental error limits, only the a-axis data are plotted. For purposes of clarity, some data circles were omitted from the curves, but all data points were used in determining the curve shapes, and a complete tabulation of the data is given in the appendix.

The residual resistivity of the a-axis crystal was 3.50

Figure 20. Electrical resistivity, residual subtracted, as a function of temperature for the a- and c-axis crystals and for a polycrystalline sample. The solid line gives the predicted polycrystalline behavior from an averaging of a- and c-axis single crystal data.
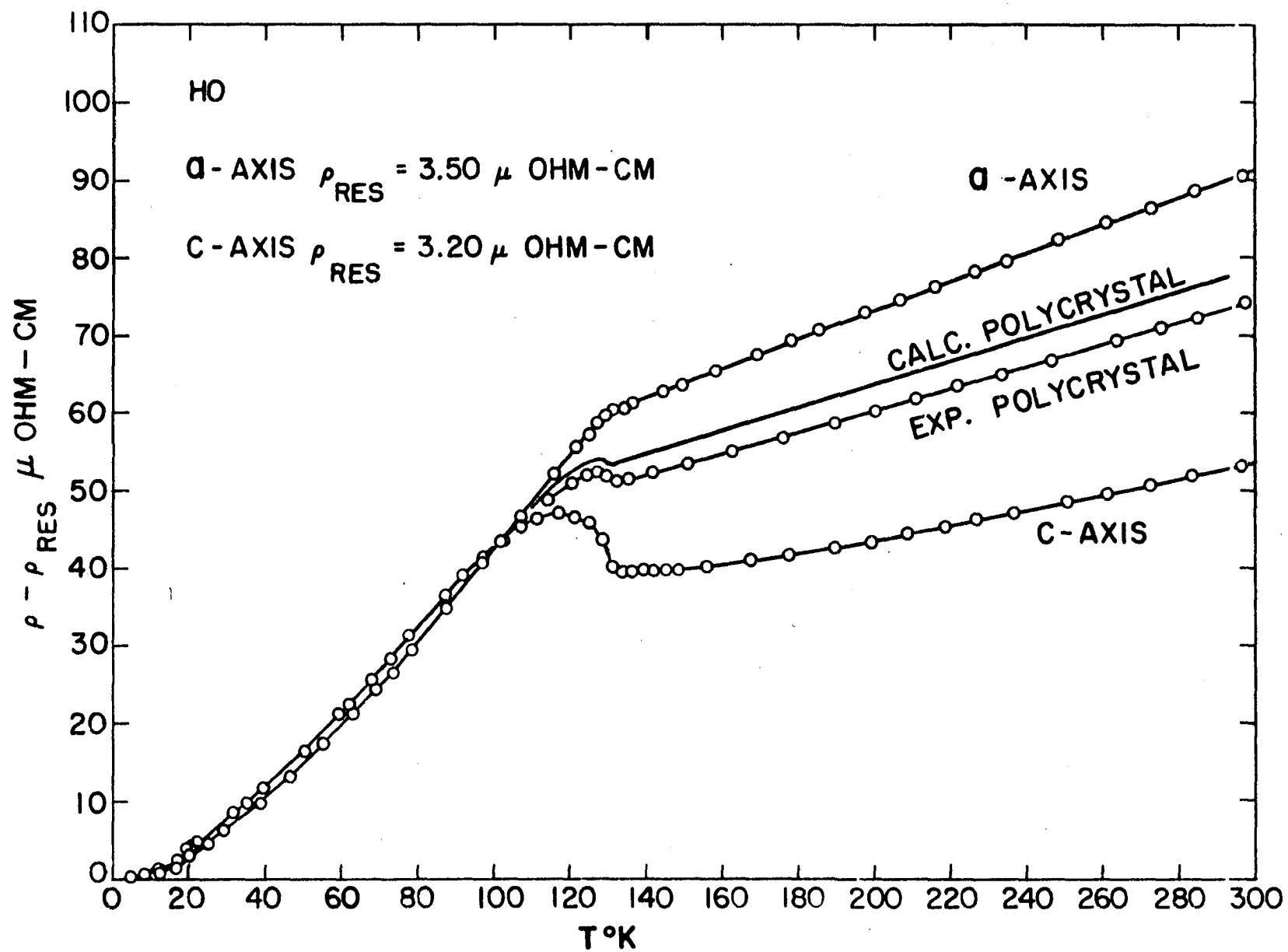
μohm-cm. The potential probes were 5.83 mm apart and were centered on the crystal, which had a length of 10.5 mm. The current contacts were within one millimeter of each end. Resistivity measurements on the a-axis crystal were made at increasing temperatures from 77.4°K to room temperature. Measurements at decreasing temperatures from room temperature to 125.4°K were next made to check for thermal hysteresis at the Néel point. All data points fell on the same curve. A final series of measurements was then taken at increasing temperatures from 4.6°K to 78.4°K.

Figure 21 is an expanded view of the region near the Néel point. Data for both increasing and decreasing temperatures are displayed in a plot of $(\rho - \rho_{res})^2$ versus T, and no thermal hysteresis is observable. At 132°K the curve of the a-axis crystal first begins to deviate (with decreasing temperatures) from its almost linear behavior observable at higher temperatures. This is taken as the Néel point.

A very slight change of slope occurred at approximately 20°K.

The residual resistivity of the $\langle 10\bar{1}0 \rangle$ crystal was 3.60 μohm-cm. The potential probes were 5.24 mm apart and were centered on the crystal, which had a length of 9.0 mm. Resistivity measurements were made at increasing temperatures from 78.2°K to 153°K, at decreasing temperatures from 153°K to 124.8°K, and at increasing temperatures from 124.8°K to

Figure 21. An expanded plot of $(\rho - \rho_{res})^2$ versus temperature for the a-axis and c-axis crystals in the vicinity of the Néel point.
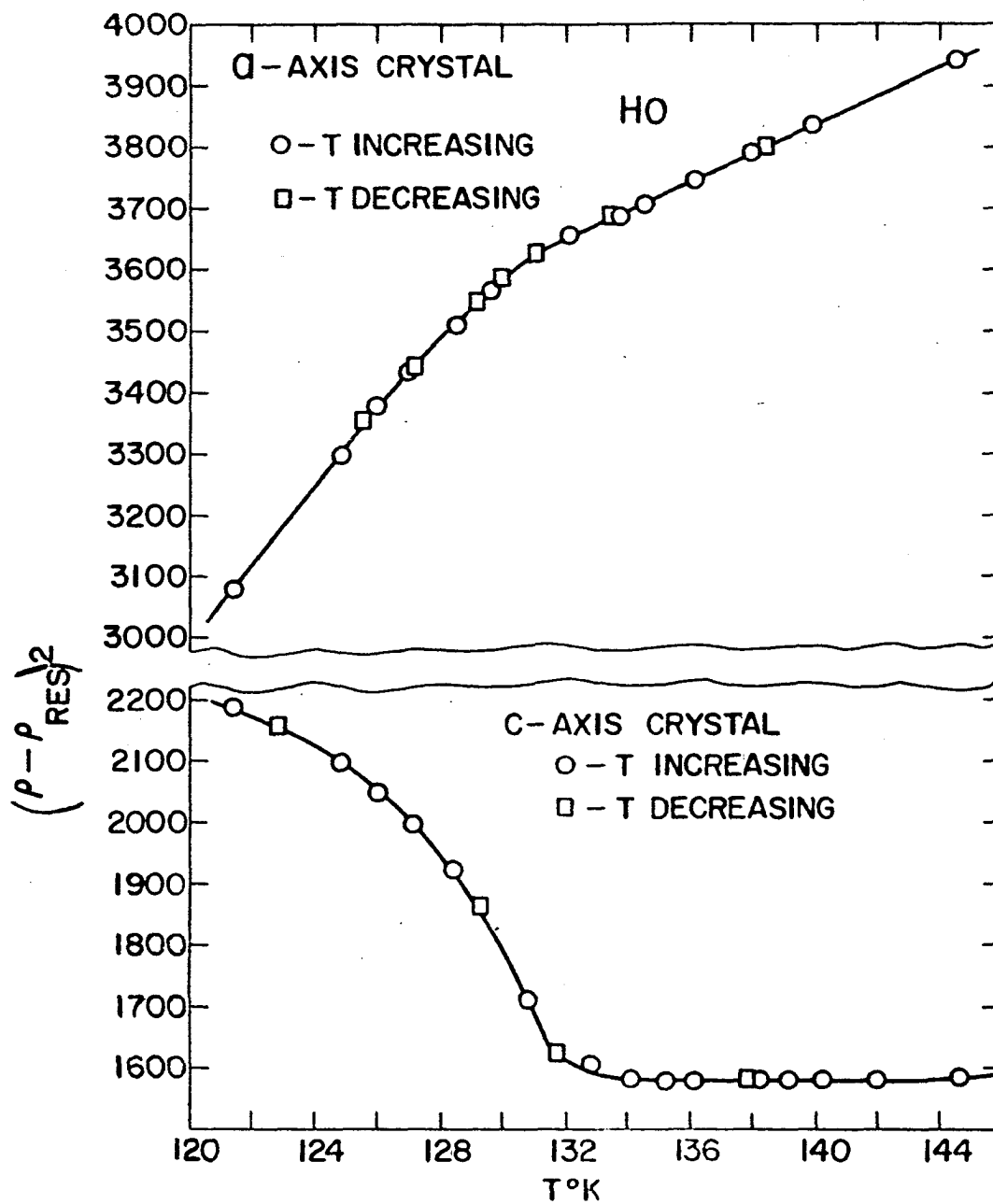
296.3°K. Measurements were then taken at increasing temperatures from 4.2°K to 155.1°K.

The data for the ⟨10$\bar{1}$0⟩ crystal are tabulated in the appendix. The plot of a-axis data shown in Figure 20 displays the temperature variation of the resistivity quite well, as the differences between the a-axis data and the ⟨10$\bar{1}$0⟩ direction data can be attributed to the experimental errors involved. No thermal hysteresis was indicated at the Néel point, which was taken as 132°K. Just as in the a-axis data, a small change of slope occurred at 20°K.

The residual resistivity of the c-axis crystal was 3.20 μohm-cm. The crystal was 9.8 mm long, and the potential probes were 5.83 mm apart. Resistivity measurements were made at increasing temperatures from 77.9°K to 296.0°K, at decreasing temperatures from 296.1°K to 122.8°K, and from 4.3°K to 87.6°K. An attempt was made to check the change in slope at 20°K for thermal hysteresis. Measurements were made at decreasing temperatures from 29°K to 12°K, at increasing temperatures from 12°K to 29°K, and at decreasing temperatures from 29°K to 19°K. At most, only a very small amount of hysteresis was indicated, and the difference between curves could be attributed to experimental error. A resistivity difference of only 0.3 μohm-cm at 20°K was obtained for the two most widely separated curves. The data are tabulated in the appendix.

Figure 21 shows the marked minimum in resistivity which occurred at the Néel point for the c-axis crystal. A temperature of 132°K is taken as the Néel point, although the essentially temperature-independent nature of the curve from 132°K to 150°K indicates that the effects of magnetic ordering may extend well above the Néel temperature.

Also plotted in Figure 20 is a curve of polycrystalline holmium data determined by Colvin, et al. (6) and a curve of calculated polycrystalline data which were obtained from the single crystal data by the use of Voigt's rule,

$$\rho_{poly} = \frac{2\rho_a + \rho_c}{3} \tag{5.2}$$

where ρ_a is the a-axis resistivity, ρ_c is the c-axis resistivity, and ρ_{poly} is the calculated resistivity of a polycrystalline sample. This relationship has been verified for the hexagonal rare earth yttrium by Alstad, et al. (65).

VI. DISCUSSION

A. Magnetic Measurements

The magnetic properties of holmium were found to be anisotropic over the entire temperature range covered in this investigation. The existence of magnetic anisotropy in the paramagnetic region has been shown experimentally in erbium by Green, et al. (12) and in dysprosium by Behrendt, et al. (10). The anisotropy for the case of holmium is displayed in Figure 12. No anisotropy was observed in the basal plane at temperatures above 100°K. This is in agreement with the work of Boas and Mackenzie (52), since X is a linear function of H above 100°K. $\frac{1}{X}$ values for c-axis data are higher than basal plane values, which indicates that the c-axis is the direction of hard magnetization. Paramagnetic Curie temperatures, Θ_p, are obtained from extrapolations of the straight line portions of the plots. For the basal plane, $\Theta_p = 88°K$; and for the c-axis, $\Theta_p = 73°K$. Since the Curie temperature for a polycrystalline material is proportional to an effective exchange integral, Behrendt (56) has proposed that the anisotropy in the paramagnetic region may be due to anisotropic exchange integrals arising from anisotropic crystalline fields.

The Curie constant, C_g, in Equation 2.14 for the effective paramagnetic moment,

$$\mathrm{eff} = 2.83 \sqrt{AC_g} \,, \tag{2.14}$$

is given by the slopes of the straight lines of Figure 12.

Since the straight lines are essentially parallel, μ_{eff} = 11.2 Bohr magnetons for all three crystalline directions. The data reported by Rhodes, et al. (9) for polycrystalline holmium give a slightly different slope and an effective moment of 10.9 Bohr magnetons. The theoretical value of μ_{eff} is given by Equation 2.13,

$$\mu_{eff} = g\left[J(J+1)\right]^{1/2} . \qquad (2.13)$$

Substituting the values of g = 5/4 and J = 8, which are obtained when the ground state of $^{5}I_{8}$ is assumed, one obtains μ_{eff} = 10.6 Bohr magnetons. It should be noted that the results of Green, et al. (12) for erbium also gave experimental values of μ_{eff} which were approximately three per cent higher than those predicted by this simple theory.

The a-axis and the <10$\bar{1}$0> crystal data show the existence of a Néel point at 132°K. It can be seen in Figure 9 that the Néel temperature is field dependent and decreases with increasing magnetic field. Below 132°K, the a-axis and the <10$\bar{1}$0> crystal data indicate that the sample is in an antiferromagnetic state. However, there is no indication of antiferromagnetism in the c-axis data plotted in Figure 19. These results agree with the neutron diffraction studies of Cable, et al. (32) who suggested that below 132°K the magnetic moments had in the absence of an external field an antiferromagnetic helical spin arrangement with the magnetic moments lying in the basal plane.

At very low temperatures, the $\langle 10\bar{1}0 \rangle$ direction is the direction of easy magnetization. The determinations of the saturation moments, $\sigma_{\infty,0}$, for the a-axis and the $\langle 10\bar{1}0 \rangle$ crystals are shown in Figures 10 and 11. For the $\langle 10\bar{1}0 \rangle$ crystal, the $T^{3/2}$ plot gives a somewhat better fit. This is in agreement with the theoretical results of Kasuya (23) and Bloch (24), but not with those of Niira (26), who obtained a T^2 dependence for single crystals of dysprosium. However, if only temperatures of $20°K$ and under are considered, the plots are about equally good.

For the $\langle 10\bar{1}0 \rangle$ crystal, $\sigma_{\infty,0} = 350.2 \pm 3.5$ cgs units per gram, and $N_{eff} = 10.34 \pm 0.15$ Bohr magnetons. For the a-axis crystal, $\sigma_{\infty,0} = 306.0 \pm 3.1$ cgs units per gram, and $N_{eff} = 9.00 \pm 0.09$ bohr magnetons. A theoretical determination of the saturation moment from Equation 2.16 gives $N_{eff} = gJ = 10$ Bohr magnetons, so that slightly more than the total moment predicted by Equation 2.16 is obtained in the $\langle 10\bar{1}0 \rangle$ direction. The additional moment may arise from the contribution of polarized conduction electrons which were not considered in the derivation of Equation 2.16.

If the saturation moment of the $\langle 10\bar{1}0 \rangle$ crystal is multiplied by the cosine of $30°$, a value of 8.95 bohr magnetons is obtained. This is equal, within the limits of experimental error, to the saturation moment of the a-axis crystal. Since the a-axis and the $\langle 10\bar{1}0 \rangle$ directions are $30°$

apart in the basal plane, a reasonable interpretation of this
result is that although the external magnetic field is
directed along an a-axis, the magnetic moments at saturation
are lying along the easy <$10\bar{1}0$> directions located 30° on
either side of the a-axis; and only their components in the
direction of the field contribute to the magnetization.
Because of the anisotropy effects involved, the approach to
saturation of the a-axis magnetic moment need not be expected
to follow either type of temperature dependence.

The a-axis and the <1010> crystal magnetization curves
at lowest temperatures have the characteristic shape of
curves for ferromagnetic materials, and the decreasing field
measurements show a considerable amount of hysteresis.
Neutron diffraction results of Cable, et al. (32) also
showed that ferromagnetism could be induced in holmium at
temperatures below 20°K by the application of a magnetic
field in the basal plane.

Curves for the c-axis crystal are quite different. The
spontaneous magnetization of about 60 cgs units per gram, or
1.7 Bohr magnetons per atom, followed by a very flat magneti-
zation curve agrees quite well with the neutron diffraction
results of Koehler.[1] His results indicate that below 20°K in
zero magnetic field a small component (about 2 Bohr magnetons)

[1]Koehler, W. C. Oak Ridge National Laboratory, Oak
Ridge, Tenn. Concerning neutron diffraction data on holmium.
Private communication. (1960).

of the magnetic moment is directed along the c-axis in a ferromagnetic alignment, while the basal plane orientation remains a spiral. It is extremely difficult to turn the moments further away from the basal plane by the application of a magnetic field along the c-axis.

The antiferromagnetic range extends from slightly below 20°K to 132°K. The anomalous behavior at low fields near 20°K shown by the inset of Figure 8 and the "knees" in the magnetization curves show that holmium is more complex than erbium or dysprosium for which no such effects were obtained. An extrapolation to zero field of a plot of the critical fields at which the discontinuities in the magnetization curves first occurred versus temperature was used by Behrendt, et al. (10) and Green, et al. (12) to determine the ferromagnetic-antiferromagnetic transition temperatures. A value of 15°K was obtained when this method was applied to holmium, but the complex behavior of the magnetization curves in the vicinity of 20°K casts some doubt on the relevance of this value.

B. Resistivity Measurements

The ratio of electrical resistivity values for two different crystal directions is a measure of the anisotropy of the resistivity. At room temperature, $\frac{\rho_a}{\rho_c} = 1.70$ and $\frac{\rho_a}{\rho_{<10\bar{1}0>}} = 0.98$. ρ_a, $\rho_{<10\bar{1}0>}$, and ρ_c are the

resistivities along the a-axis, the <$10\bar{1}0$>, and the c-axis
directions. At temperatures above 200°K, the plots of
ρ - ρ_{res} versus temperature are essentially linear, and the
slopes of these plots are also indicative of the degree of
anisotropy. The slope of the ρ_c curve is 0.099 μohm-cm/°K,
while the slope of the ρ_a curve is 0.176 μohm-cm/°K, and
the slope of the $\rho_{<10\bar{1}0>}$ curve is 0.184 μohm-cm/°K. It is
possible to attribute the difference in the slopes of the ρ_a
and $\rho_{<10\bar{1}0>}$ curves to experimental error. This comparison
of room temperature resistivity values and of the slopes of
the curves shows that there is at most a very small anisotropy
of the resistivity in the basal plane. These results substan-
tiate the predictions of Boas and Mackenzie (52), who suggested
that there would be no anisotropy of electrical resistivity in
the basal plane for a hexagonal close-packed crystal. The
results show a large degree of anisotropy between the a- and
c-axis directions, however.

If the large anisotropy which is observed between ρ_a and
ρ_c in the temperature region above 132°K were due to phonon
effects, it would be reasonable to expect that the extrapo-
lated-linear portions of the curves would intersect at zero
degrees Kelvin. Since the curves do not intersect, the
anisotropy is probably due to anisotropy in magnon scattering.

Calculated data for a polycrystalline sample obtained by
suitably averaging the a- and c-axis data are plotted in

Figure 20. In the paramagnetic temperature range, the curve
of resistivity versus temperature is linear, and the slope of
the curve is 0.147 μ ohm-cm/°K. The experimentally deter-
mined data of Colvin, et al. (6) for polycrystalline holmium
are also plotted and the slope of this curve is 0.144 μ ohm-
cm/°K. The two curves also show the same shape in the
vicinity of the Néel point. It has been pointed out in
Chapter I that "polycrystalline" samples of rare earth metals
often have some degree of preferred orientation so that
perfect agreement is not expected.

The magnetic measurements indicated that 132°K is the
Néel temperature for holmium. A "knee" occurs in the curves
of ρ_a and $\rho_{<10\bar{1}0>}$ at this temperature. The slopes of the
curves decrease but remain positive.

The curve of ρ_c has a broad unsymmetrical peak with a
maximum at 116°K followed by a minimum at 132°K, the Néel
temperature. Green, et al. (12) have suggested that this
peak indicates that the ordering of the spins in the
antiferromagnetic-paramagnetic transition occurs over a wide
temperature range. The temperature-independent nature of the
c-axis resistivity from 132°K to 150°K may also indicate that
ordering effects extend well into the paramagnetic range.

Plots of ln T versus ln($\rho - \rho_{res}$) for the a- and c-axis
crystals are displayed in Figure 22 in order to show the
temperature dependence of the resistivity below the Néel

Figure 22. Plot of Ln $(\rho - \rho_{res})$ versus Ln T for the a-axis and c-axis crystals.
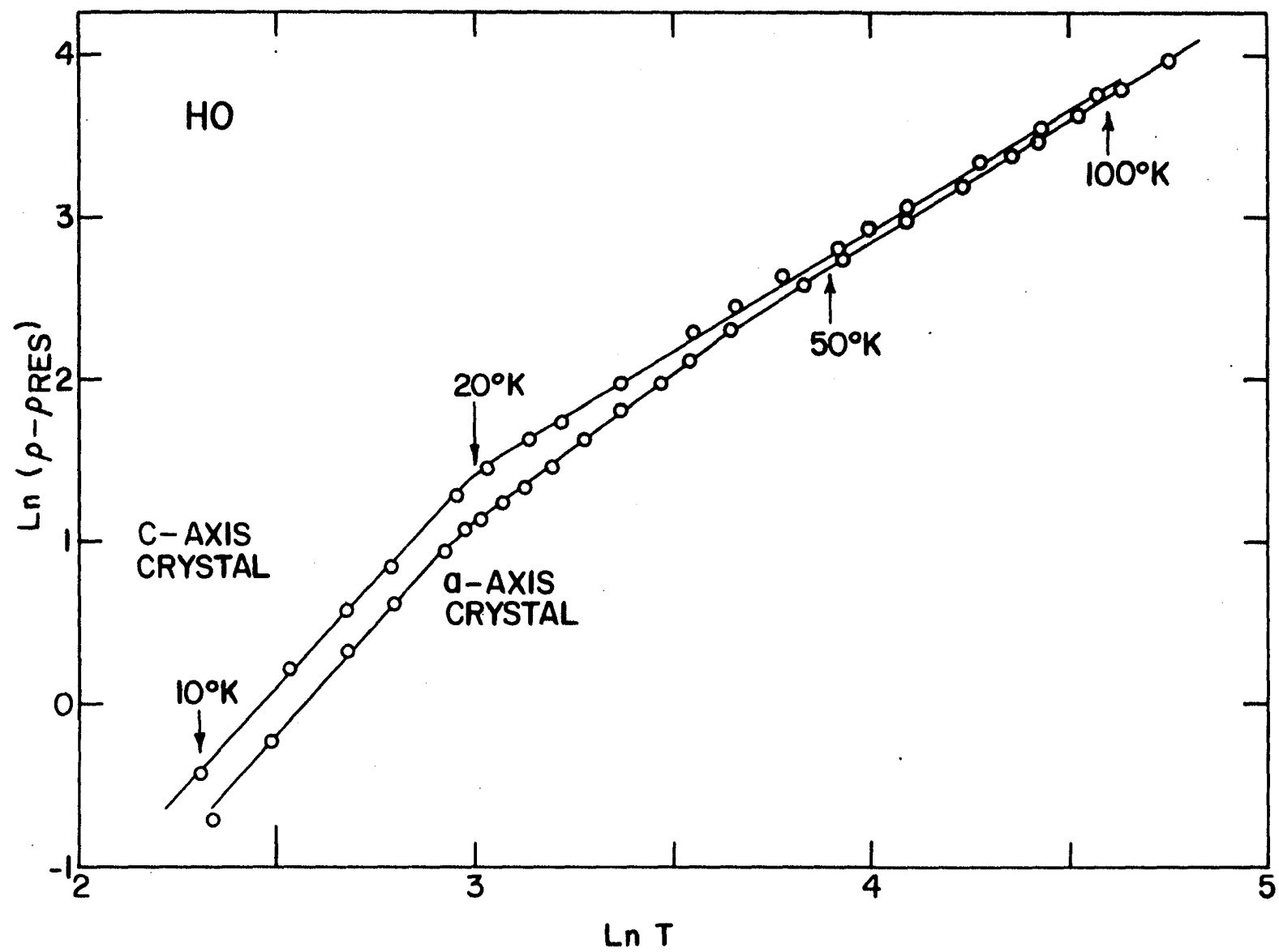
point. The c-axis data have a $T^{3/2}$ dependence from 100°K to 20°K where a rather sharp transition to a $T^{8/3}$ dependence occurs. The a-axis data are seen to approach the same temperature dependences shown by the c-axis data above and below 20°K, but the transition from $T^{3/2}$ to $T^{8/3}$ is much more gradual and extends from approximately 15°K to 40°K. It is felt that care must be taken in considering the data below 10°K since $\dfrac{\rho - \rho_{res}}{\rho_{res}} \leq 0.1$, and the temperature dependence of the residual resistivity may make a substantial contribution to the total resistivity.

A magnetic transition near 20°K has been discussed in Chapter IV, Section A. The effects of the transition on the resistivity are much more apparent for the c-axis crystal than for the a-axis crystal. This was also true for erbium, which displayed a discontinuous jump in the c-axis resistivity data at the magnetic transition temperature. No anomalous effect was observed in the erbium a-axis data at this temperature.

The resistivity data of Green, et al. (12) for single crystals of erbium and of Hall, et al. (13) for single crystals of dysprosium also give ρ_c curves which have a peak just below the Néel temperature and ρ_a curves which have only a change in slope. (The ρ_a and ρ_c data of Hall are predicted values obtained from measurements on a poly-crystalline sample, a single crystal oriented 18.2° from the c-axis, and a single crystal oriented 42.0° from the

c-axis.) The resistivity curves of dysprosium, holmium, and
erbium are rather similar in the paramagnetic range as well.
In each case, at room temperature, ρ_a is more than fifty per
cent greater than ρ_c. The similarity of resistivity
properties of the three metals in the paramagnetic region
suggests that their magnetic properties might also have much
in common.

Kasuya (48) obtained an equation in which the magnetic
part of the resistivity in the paramagnetic region is
proportional to the square of the effective exchange integral.
Behrendt (56) explained the anisotropy of the magnetic
susceptibility in the paramagnetic region, which is charac-
terized by different paramagnetic Curie temperatures for
different crystal directions, as being due to an anisotropic
exchange integral. Since the paramagnetic Curie temperature
is proportional to the exchange integral for polycrystalline
materials, Hall, et al. (13) suggested that

$$\frac{\rho_{\parallel}}{\rho_{\perp}} = \left(\frac{\Theta_{p\parallel}}{\Theta_{p\perp}}\right)^2 \qquad (6.1)$$

where $\rho_{\parallel}$ and $\rho_{\perp}$ are the magnetic contributions to the
c-axis and the basal plane resistivities, while $\Theta_{p\parallel}$ and $\Theta_{p\perp}$
are the c-axis and the basal plane paramagnetic Curie
temperatures.

For dysprosium, $\dfrac{\rho_{\parallel}}{\rho_{\perp}}$ = 0.8 while $\left(\dfrac{\Theta_{p\parallel}}{\Theta_{p\perp}}\right)^2$ = 0.52. The
agreement, while not good, is promising. Using the holmium

data of this investigation, one obtains $\frac{\rho_{\parallel}}{\rho_{\perp}} = 0.62$ and $\left(\frac{\Theta_{p\parallel}}{\Theta_{p\perp}}\right)^2 = 0.69$. This agreement is rather good. However, when Equation 6.1 is applied to erbium, radical disagreement is obtained. For erbium, $\frac{\rho_{\parallel}}{\rho_{\perp}} = 0.42$ while $\left(\frac{\Theta_{p\parallel}}{\Theta_{p\perp}}\right)^2 = 3.6$. If one inverts $\left(\frac{\Theta_{p\parallel}}{\Theta_{p\perp}}\right)^2$, however, one obtains a value of 0.28. If this value is compared with $\frac{\rho_{\parallel}}{\rho_{\perp}}$, it is seen that the agreement is about the same as in the case of dysprosium. It should be noted that the basal plane contains the direction of easiest magnetization for holmium and dysprosium, and $\Theta_{p\parallel}$ is less than $\Theta_{p\perp}$. For erbium, however, the direction of easiest magnetization is the c-axis and $\Theta_{p\parallel}$ is greater than $\Theta_{p\perp}$. Equation 6.1, which was obtained from a theoretical treatment for polycrystalline material, is probably too simple an approach. It is evident that experimental data on single crystals of other rare earth metals as well as a theoretical treatment which considers the effects of spin-orbit coupling and anisotropy, which Kasuya neglected, are needed to explain the relationship between the magnetic and electrical resistivity properties of the rare earths.

VII. LITERATURE CITED

1. Spedding, F. H., Legvold, S., Daane, A. H., and Jennings, L. D. Some physical properties of the rare earth metals. In Gorter, C. J., ed. Progress in low temperature physics. Vol. 2. pp 368-394. Amsterdam, the Netherlands, North-Holland Publishing Company. 1957.

2. Van Vleck, J. H. The theory of electric and magnetic susceptibilities. London, England, Oxford University Press. 1932.

3. Rhodes, B. L. Magnetic properties of holmium and thulium. Unpublished M.S. Thesis. Ames, Iowa, Library, Iowa State University of Science and Technology. 1953.

4. Joos, G. The magnetism of the rare earth metals. In Dillinger, J. R., ed. Low temperature physics and chemistry. pp 581-583. Madison, Wisc., the University of Wisconsin Press. 1958.

5. Herrmann, K. W. Some physical-metallurgical properties of scandium, yttrium, and the rare earth metals. Unpublished Ph.D. Thesis. Ames, Iowa, Library, Iowa State University of Science and Technology. 1955.

6. Colvin, R. V., Legvold, S., and Spedding, F. H., Phys. Rev. 120, 741 (1960).

7. Gerstein, B. C., Griffel, M., Jennings, L. D., and Miller, R. E., J. Chem. Phys. 27, 394 (1957).

8. Born, H. J. Low temperature thermoelectric power of the rare earth metals. Unpublished Ph.D. Thesis. Ames, Iowa, Library, Iowa State University of Science and Technology. 1960.

9. Rhodes, B. L., Legvold, S., and Spedding, F. H., Phys. Rev. 109, 1547 (1958).

10. Behrendt, D. R., Legvold, S., and Spedding, F. H., Phys. Rev. 109, 1544 (1958).

11. _____, and _____, Phys. Rev. 106, 723 (1957).

12. Green, R. W., Legvold, S., and Spedding, F. H. Magnetization and electrical resistivity of erbium single crystals. Phys. Rev. (to be published ca. 1961).

13. Hall, P. M., Legvold, S., and Spedding, F. H., Phys. Rev. 116, 1446 (1959).

14. Hall, P. M., Legvold, S., and Spedding, F. H., Phys. Rev. 117, 971 (1960).

15. Van Vleck, J. H., Am. J. Phys. 18, 495 (1950).

16. Dekker, A. J. Solid state physics. Englewood Cliffs, N.J., Prentice-Hall, Inc. 1957.

17. Wilson, A. H. The theory of metals. 2nd ed. London, England, Cambridge University Press. 1958.

18. Weiss, P., J. de Physique 6, 661 (1907).

19. Langevin, P., J. de Physique 4, 619 (1905).

20. Heisenberg, W., Z. Physik 49, 619 (1928).

21. Stoner, E. C., Rep. Progr. Phys. 11, 43 (1948).

22. Zener, C., Phys. Rev. 81, 440 (1951).

23. Kasuya, T., Progr. Theoret. Phys. (Kyoto) 16, 45 (1956).

24. Bloch, F., Z. Physik 61, 206 (1930).

25. de Gennes, P. G., Compt. rend. 247, 1936 (1958).

26. Niira, Kazuo, Phys. Rev. 117, 129 (1960).

27. Liu, S. H., Behrendt, D. R., Legvold, S., and Good Jr., R. H., Phys. Rev. 116, 1464 (1959).

28. Yoshinori, A., J. Phys. Soc. Japan 14, 807 (1959).

29. Villain, J., Phys. and Chem. Solids 11, 303 (1959).

30. Koehler, W. C., Neutron diffraction by helical spin structures. Acta. Cryst. (to be published ca. 1961).

31. Herpin, A. and Meriel, P., Compt. rend. 250, 1450 (1960).

32. Cable, J. W., Child, H. R., Koehler, W. C., Wilkinson, M. K., and Wollan, E. O., Neutron diffraction studies of rare earth metals and compounds. Paper presented at International Atomic Energy Agency Symposium on Pile Neutron Research and Physics, Vienna, Austria. Oct. 17-18, 1960. (Multilith) Oak Ridge, Tenn., Oak Ridge National Laboratory. 1960.

33. Bardeen, J., J. Appl. Phys. 11, 88 (1940).

34. Bloch, F., Z. Physik 52, 555 (1928).

35. Jones, H. Theory of electrical conductivity in metals. In Flugge, S., ed. Handbuch der Physik. Band 19, pp 227-315. Berlin, Germany, Springer. 1956.

36. Matthiessen, A. and Vogt, C., Ann. Phys. und Chem. Ser. 2, 122, 19 (1864).

37. MacDonald, D. K. C. Electrical conductivity of metals and alloys at low temperatures. In Flugge, S., ed. Handbuch der Physik. Band 14, pp 137-197. Berlin, Germany, Springer. 1956.

38. Gerritsen, A. N. Metallic conductivity, Experimental part. In Flugge, S., ed. Handbuch der Physik. Band 19, pp 137-226. Berlin, Germany, Springer. 1956.

39. Gruneisen, E., Ann. Physik 16, 530 (1933).

40. Bloch, F., Z. Physik 59, 208 (1930).

41. Sondheimer, E. H., Proc. Roy. Soc. (London) A 203, 75 (1950).

42. Blackman, M., Proc. Phys. Soc. (London) 64A, 681 (1951).

43. MacDonald, D. K. C. and Mendelssohn, K., Proc. Roy. Soc. (London) A 202, 523 (1950).

44. Mott, N. F., Proc. Roy. Soc. (London) A 153, 669 (1936).

45. Wilson, A. H., Proc. Roy. Soc. (London) A 167, 580 (1938).

46. Ziman, J. M. Electrons and phonons. London, England, Oxford University Press. 1960.

47. White, G. K. and Woods, S. B., Phil. Trans. A 251, 273 (1959).

48. Kasuya, T., Progr. Theoret. Phys. (Kyoto) 16, 58 (1956).

49. de Gennes, P. G. and Friedel, J., Phys. Chem. Solids 4, 71 (1958).

50. Turov, E. A., Bull. Acad. Sci. USSR. Phys. Ser. (English Translation) 19, 426 (1955).

51. Kondorsky, E., Galkina, O. S. and Tchernikova, L. A., J. Appl. Phys. 29, 243 (1958).

52. Boas, W. and Mackenzie, J. K. Anisotropy in metals. In Chalmers, B., ed. Progress in metal physics. Vol. 2, pp 90-120. New York, N.Y., Interscience Publishers, Inc. 1950.

53. Baroody, E. M., Phys. Rev. 58, 793 (1940).

54. Spedding, F. H. and Powell, J. E., J. Metals 6, 1131 (1954).

55. _____ and Daane, A. H., J. Metals 6, 504 (1954).

56. Behrendt, D. R. Magnetic properties of neodymium and dysprosium single crystals. Unpublished Ph.D. Thesis. Ames, Iowa, Library, Iowa State University of Science and Technology. 1956.

57. Greninger, A. B., Trans. Am. Inst. Mining, Met. Engrs. 117, 61 (1935).

58. Sucksmith, B., Phil. Mag. 8, 158 (1929).

59. Thoburn, W. C. Magnetic properties of Gd-La and Gd-Y alloys. Unpublished Ph.D. Thesis. Ames, Iowa, Library, Iowa State University of Science and Technology. 1956.

60. Bozorth, R. M. Ferromagnetism. New York, N.Y., D. Van Nostrand Company, Inc. 1951.

61. Elliott, J. F. The ferromagnetic properties of the rare earth metals. Unpublished Ph.D. Thesis. Ames, Iowa, Library, Iowa State University of Science and Technology. (1953).

62. Henry, W. E. and Dolecek, R. L., Rev. Sci. Instr. 21, 496 (1950).

63. Anderson, G. S., Legvole, S., and Spedding, F. H., Phys. Rev. 109, 243 (1958).

64. Arajs, S. and Miller, S. D. Spontaneous magnetization of some gadolinium alloys. (Multilith) U. S. Steel Corp., Edger C. Bain Laboratory for Fundamental Research, Report No. 821. (1959).

65. Alstad, J. K., Colvin, R. V., and Legvold, S. Single and polycrystal resistivity relationships for yttrium. Phys. Rev. (to be published ca. 1961).

66. Thoburn, W. C., Rev. Sci. Instr. 29, 990 (1958).

VIII. ACKNOWLEDGMENTS

The author also wishes to express his deepest gratitude to his wife for her encouragement and understanding during the years of graduate study.

IX. APPENDICES

A. Tabulation of the Magnetic Data[a]

Table 1. Experimental data for the a-axis crystal

σ	H	σ	H	σ	H
1.8°K (80°K)		**4.2°K (298°K)**		**10.0°K (298°K)**	
3.23	0.50	4.72	0.50	4.75	0.51
68.63	0.88	20.08	0.96	38.78	0.93
247.1	1.56	278.4	2.50	234.0	1.07
295.4	5.47	291.5	4.48	262.0	1.53
300.8	8.46	299.0	7.46	278.9	2.50
303.2	11.45	301.1	9.46	290.5	4.18
304.4	14.45	302.8	11.45	294.9	5.47
305.0	17.45	303.9	14.45	300.9	8.46
		304.5	17.45	302.9	11.45
303.4	11.8			304.1	14.45
302.3	9.8			304.4	17.45
301.8	7.7				
295.0	4.6				
286.9	2.6				
12.0°K (298°K)		**14.5°K (298°K)**		**17.3°K (298°K)**	
3.64	0.50	4.07	0.50	3.82	0.49
6.15	0.74	6.00	0.99	4.55	0.73
12.35	1.03	9.55	1.21	6.19	0.99
207.3	1.13	89.60	1.34	10.12	1.22
238.7	1.32	192.4	1.41	15.29	1.47
252.3	1.55	234.5	1.58	23.67	1.73
260.5	1.80	245.4	1.80	126.15	1.77
265.9	2.02	255.9	2.04	198.41	1.88
270.3	2.24	268.7	2.57	233.62	2.08
275.0	2.50	281.3	3.54	257.37	2.54
284.7	3.49	288.0	4.48		
289.8	4.48	292.4	5.47		
299.1	7.46	297.3	7.46		
302.7	11.46	300.2	9.59		
303.8	14.45	301.9	11.46		
304.1	17.45	303.5	14.45		
		303.7	17.45		

[a]Temperatures in parentheses are annealing temperatures.

108

Table 1. (Continued)

19.0°K (298°K)

σ	H
7.6	0.49
13.8	0.98
16.45	1.38
20.59	1.96
151.9	2.33
234.6	2.58
268.6	3.52
281.8	4.54
288.2	5.48
294.7	7.47
298.1	9.47
300.3	11.46
302.1	14.46
302.4	17.46

22.2°K (298°K)

σ	H
7.57	0.49
12.45	0.98
15.16	1.47
17.27	1.97
18.78	2.47
19.41	2.72
20.91	2.96
22.85	3.21
60.97	3.39
160.5	3.46
221.9	3.60
238.9	3.80
265.1	4.52
280.2	5.50
289.8	6.98
294.2	8.47
299.0	11.46
300.8	14.46
301.3	17.46

24.6°K (37°K)

σ	H
6.51	0.99
13.77	1.98
19.43	2.97
21.20	3.45
23.82	3.96
28.12	4.20
106.0	4.31
178.9	4.38
231.3	4.58
246.3	4.81
255.6	5.04
262.4	5.28
267.3	5.52
275.4	6.00
280.9	6.49
291.8	8.48
297.6	11.46
299.8	15.46
300.5	17.46

30.0°K (78°K)

σ	H
4.33	0.99
11.18	2.98
18.50	4.96
20.43	5.46
23.72	5.96
28.76	6.20
84.33	6.35
108.9	6.52
148.43	6.73
229.8	6.84
244.12	7.06
259.93	7.53
268.75	8.02
275.0	8.50
284.3	9.49
290.5	10.98

35.0°K (20°K)

σ	H
3.96	0.99
10.32	2.98
13.39	3.98
16.86	5.02
18.38	5.48
20.12	5.96
22.10	6.52
25.00	7.14
32.73	7.54
92.78	7.83
119.8	8.27
182.5	8.63
262.2	9.53
277.8	10.57
284.3	11.49
293.3	14.47
296.0	17.47

37.5°K (10°K)

σ	H
4.15	0.99
7.43	1.98
10.53	2.98
16.94	4.96
18.57	5.48
20.12	5.96
22.23	6.64
24.51	7.30
27.45	7.96
39.32	8.37
109.88	8.80
133.44	9.26
217.40	9.62
275.04	11.50

Table 1. (Continued)

σ	H	σ	H	σ	H
40.4°K (50°K)		**45.0°K (37.5°K)**		**50.0°K (35°K)**	
3.30	0.99	4.15	0.99	3.35	0.99
9.31	2.98	9.71	2.98	8.65	2.98
15.31	4.97	18.40	5.97	16.95	5.97
24.56	7.96	27.75	8.95	22.40	7.98
26.58	8.46	40.19	9.93	25.16	8.95
42.91	8.92	126.9	10.84	28.24	9.95
81.55	9.08	249.7	11.55	42.98	11.01
105.8	9.35	264.2	12.61	94.97	11.36
113.1	9.56	278.6	14.50	117.0	11.79
121.0	9.78	285.6	17.49	163.1	12.26
152.5	7.99	255.4	11.8	229.3	12.68
213.7	10.12	195.9	11.0	254.5	13.58
245.60	10.56	115.5	10.1	265.9	14.52
259.5	11.03	74.8	9.1	272.5	15.52
268.1	11.52	30.9	8.2	278.6	17.50
273.7	12.00	20.5	6.2		
280.7	12.99	10.0	3.1		
286.2	14.48				
290.3	17.48				
56.5°K (24.6°K)		**61.8°K (22°K)**		**61.8°K (22°K)**	
8.25	2.99	3.05	0.99	243.8	16.56
15.88	5.97	7.77	2.99	252.8	17.54
23.58	8.96	15.01	5.98	221.8	15.5
32.57	11.94	22.20	8.96	164.0	15.0
41.60	12.43	30.05	11.95	121.5	14.7
94.51	12.96	32.99	12.94	115.8	14.2
111.4	13.30	35.80	13.44	100.9	13.6
141.7	13.75	40.54	13.65	78.68	13.1
218.6	14.25	73.70	13.87	33.77	12.3
236.1	14.62	92.47	14.07	23.46	9.1
		103.4	14.32		
		110.2	14.53		
		118.1	14.79		
		137.7	15.01		
		186.+	15.17		
		210.3	15.36		
		221.9	15.83		
		235.4	16.08		

Table 1. (Continued)

σ	H	σ	H	σ	H
67.6°K (298°K)		74.0°K		77.9°K	
2.29	1.00	2.23	1.00	6.40	2.99
6.78	2.99	6.45	2.99	12.52	5.98
13.62	5.97	13.03	5.98	18.86	8.97
20.51	8.96	19.64	8.96	25.41	11.95
27.74	11.95	26.47	11.95	32.23	14.94
32.92	13.94	33.70	14.94	34.62	15.94
40.54	14.95	35.08	15.44	35.86	16.44
106.07	15.81	37.04	15.93	37.26	16.93
114.3	16.29	38.78	16.19	38.22	17.20
162.8	16.71	43.26	16.42	39.45	17.43
214.8	17.15	79.29	16.62	42.27	17.68
226.6	17.59	94.68	16.83	51.72	17.91
		102.37	17.09		
		108.82	17.32		
		111.00	17.56		
		114.5	17.80		

σ	H	σ	H	σ	H
78.9°K		79.2°K		88.9°K	
2.11	1.00	2.14	1.00	1.95	1.00
4.17	1.99	6.24	2.99	5.86	2.99
8.27	3.99	10.32	4.98	11.70	5.98
12.41	5.98	16.52	7.97	17.54	8.97
16.52	7.97	25.16	11.95	23.58	11.96
25.21	11.95	31.82	14.94	29.71	14.95
31.92	14.94	40.60	17.93	36.03	17.94
41.26	17.93				

Table 1. (Continued)

σ	H	σ	H	σ	H
99.7°K		**109.4°K**		**119.3°K**	
2.07	1.00	1.89	1.00	2.14	1.00
5.64	2.99	5.49	2.99	5.65	2.99
11.10	5.98	10.91	5.98	11.32	5.98
16.69	8.97	16.42	8.97	17.05	8.97
22.33	11.96	22.01	11.96	22.96	11.96
28.11	14.95	27.64	14.95	29.08	14.95
33.91	17.94	33.44	17.94	35.52	17.94
123.9°K		**126.0°K**		**127.4°K**	
2.07	1.00	5.96	2.99	2.26	1.00
5.84	2.99	12.02	5.98	6.16	2.99
11.72	5.98	18.17	8.97	12.34	5.98
17.71	8.97	24.75	11.96	18.70	8.97
24.06	11.96	31.70	14.94	25.47	11.95
30.70	14.94	39.63	17.93	32.89	14.94
37.94	17.93			40.97	17.93
129.0°K.		**130.4°K**		**132.0°K**	
6.19	2.99	2.17	1.00	2.07	1.00
12.60	5.98	6.36	2.99	6.22	2.99
19.13	8.97	12.84	5.98	12.49	5.98
26.20	11.95	19.44	8.97	18.70	8.97
33.27	14.94	26.10	11.95	25.05	11.95
40.04	17.93	32.66	14.94	31.31	14.94
		39.18	17.93	37.52	17.93

Table 1. (Continued)

133.0°K

σ	H
2.420	1.00
6.237	2.99
12.40	5.98
18.49	8.97
24.70	11.96
30.89	14.94
36.98	17.93

135.5°K

σ	H
1.92	1.00
6.00	2.99
11.78	5.98
17.65	8.97
23.52	11.95
29.38	14.95
35.09	17.94

140.1°K

σ	H
1.73	1.00
5.53	2.99
10.68	5.98
15.96	8.97
21.28	11.96
26.59	14.95
31.78	17.94
24.70	14.2
21.49	12.3
10.76	6.2
5.42	3.2

151.2°K

σ	H
4.47	2.99
8.89	5.98
13.31	8.98
17.70	11.97
22.10	14.96
26.40	17.95
15.43	15.4
9.18	9.2

181.1°K

σ	H
1.07	1.00
3.09	2.99
6.08	5.99
9.04	8.98
12.09	11.98
15.09	14.97
18.03	17.97
12.15	12.3
9.25	9.2
6.13	6.3

214.1°K

σ	H
0.69	1.00
2.22	3.00
4.48	5.99
6.68	8.99
8.92	11.98
11.24	14.98
13.26	17.98

251.2°K

σ	H
0.60	1.00
1.75	3.00
3.42	5.99
5.12	8.99
6.82	11.99
8.53	14.98
10.17	17.98

296.8°K

σ	H
0.94	2.00
1.78	4.00
2.69	6.00
3.59	7.99
5.43	11.99
6.72	14.99
8.09	17.99

Table 2. Experimental data for the <1010̅> crystal

1.4°K (298°K) σ	H	4.2°K (298°K) σ	H	14.5°K (50°K) σ	H	20.0°K (50°K) Run 1 σ	H	20.0°K (50°K) Run 2 σ	H	25.2°K (50°K) σ	H
4.18	0.49	4.18	0.49	4.71	0.49	19.48	1.30	9.6	0.23	2.17	.57
6.22	0.74	12.09	0.73	23.78	0.95	19.15	1.46	14.2	0.47	6.31	.99
12.62	0.96	140.6	0.75	140.9	0.98	20.72	1.71	17.1	0.72	12.59	1.98
133.7	0.99	217.9	0.83	194.1	1.12	22.86	2.01	16.6	0.97	19.03	2.96
200.0	1.11	249.7	1.01	250.4	1.26	54.48	2.14	19.2	1.46	23.18	3.46
250.6	1.26	290.0	1.43	277.9	1.46	120.1	2.27	21.3	1.71	132.0	3.74
287.6	1.69	313.9	2.39	288.3	1.69	185.0	2.39	24.96	1.95	194.1	3.87
309.0	2.40	332.9	4.35	297.6	1.92	247.4	2.52	79.94	2.09	249.3	4.01
322.6	3.37	343.1	7.34	310.2	2.40	276.1	2.73	144.1	2.22	271.8	4.22
336.4	5.34	345.7	9.33	324.7	3.37	284.2	2.95			284.2	4.45
345.3	8.33	347.4	11.32	331.5	4.35	300.6	3.41			299.8	4.91
347.3	11.32	348.5	14.32	336.1	5.34	322.5	4.37			310.1	5.40
348.3	14.32	348.3	17.32	344.2	8.33	327.2	5.36			322.4	6.37
348.3	17.32			346.5	11.32	336.7	7.34			331.7	7.85
				347.3	14.32	342.7	10.83			338.8	10.92
337.9	4.5	337.9	4.5	347.2	17.32	344.9	14.33			342.7	14.33
331.4	2.6	329.8	2.6							342.7	17.33
322.5	1.6	320.0	1.6	319.5	2.6						
296.4	0.5	291.1	0.5	301.3	1.6						
		260.0	0.0	152.9	0.8						

Table 2. (Continued)

σ	H
25.2°K (50°K)	
298.2	4.6
28.46	3.1
19.99	2.2

σ	H
30.3°K (50°K) Run 1	
8.10	1.98
14.90	3.97
20.12	4.96
207.5	5.60
234.1	5.79
263.5	5.99
280.1	6.20
286.7	6.44
302.0	6.91
315.8	7.88
327.7	9.36
334.2	11.35
338.5	14.34
339.0	17.34

σ	H
30.3°K (50°K) Run 2	
21.0	4.96
32.32	5.44
96.02	5.56
187.7	5.63

σ	H
40.3°K (50°K)	
9.88	2.98
19.02	5.96
25.06	7.95
27.06	8.45
31.85	8.94
114.1	9.28
184.9	9.39
243.8	9.52
261.6	9.74
277.3	9.96
284.9	10.19
291.4	10.43
301.2	10.91
308.1	11.40
312.8	11.89
320.9	13.37
325.9	15.36
327.9	17.36
283.5	8.6

σ	H
45.1°K (50°K)	
8.70	2.98
17.16	5.97
26.22	8.95
28.06	9.45
31.00	9.94
34.20	10.18
48.50	10.41
93.12	10.57
116.7	10.77
154.0	10.95
182.9	11.14
226.2	11.31
256.9	11.50
270.4	11.72
280.1	11.95
291.7	12.43
305.8	13.40
317.3	15.38
321.3	17.37

σ	H
49.6°K	
7.94	2.98
16.12	5.97
24.50	8.96
27.52	9.95
27.22	10.44
32.04	10.94
36.28	11.18
50.90	11.40
82.47	11.58
99.31	11.81
118.9	12.03
167.9	12.17
185.1	12.39
195.0	12.62
209.7	13.09
242.0	13.53
286.2	13.44
299.8	14.44
307.9	15.42
311.1	16.40
	17.39

Table 2. (Continued)

σ	H	σ	H	σ	H
54.8°K		60.8°K		70.1°K	

σ	H	σ	H	σ	H
8.20	2.98	7.48	2.99	7.04	2.99
15.38	5.97	14.83	5.97	13.62	5.97
23.44	8.95	22.27	8.96	20.40	8.96
33.19	11.94	30.11	11.94	27.31	11.95
43.46	12.42	33.00	12.94	32.24	13.94
68.25	12.61	35.77	13.43	35.06	14.93
91.30	12.82	53.16	13.90	36.00	15.20
103.9	13.06	83.54	14.10	37.07	15.43
122.2	13.27	96.40	14.31	38.93	15.67
169.5	13.43	105.7	14.53	44.40	15.91
186.8	13.64	119.5	14.77	70.47	16.12
196.3	13.88	158.6	14.95	90.30	16.32
202.5	14.11	183.8	15.14	98.92	16.57
207.9	14.36	193.8	15.37	105.3	16.79
211.4	14.59	201.0	15.61	127.0	17.25
218.4	15.07	210.8	16.09	185.0	17.64
222.1	15.32	217.6	16.58		
224.7	15.56	222.7	17.07		
234.2	15.80	226.3	17.56		
252.8	16.01				
269.1	16.23				
277.2	16.46				
287.3	16.94				
292.5	17.43				

σ	H	σ	H	σ	H
78.8°K		91.2°K		110.3°K	

σ	H	σ	H	σ	H
2.23	1.00	5.99	2.99	5.58	2.99
6.13	2.99	11.70	5.98	11.05	5.98
12.37	5.98	17.47	8.97	16.43	8.97
18.75	8.97	23.39	11.95	22.12	11.96
25.25	11.95	29.38	14.94	27.78	14.95
31.92	14.94	35.40	17.93	33.65	17.94
34.29	15.94				
36.82	16.93			27.96	15.4
38.68	17.56			22.29	12.3
39.28	17.65			16.72	9.2
40.61	17.92			11.04	6.2

Table 2. (Continued)

σ	H	σ	H	σ	H
120.0°K		130.0°K		140.3°K	
5.74	2.99	6.54	2.99	5.63	2.99
11.30	5.98	13.00	5.97	10.59	5.98
17.13	8.97	19.46	8.96	15.96	8.97
23.18	11.95	25.98	11.95	21.23	11.96
29.47	14.94	32.40	14.94	26.51	14.95
36.12	17.93	38.93	17.92	31.64	17.94
160.8°K		188.6°K		219.1°K	
3.86	2.99	.88	1.00	.54	1.00
7.74	5.96	2.94	2.99	2.33	3.00
11.47	8.98	5.69	5.99	4.50	5.99
15.31	11.97	8.45	8.98	6.56	8.99
19.12	14.97	11.20	11.98	8.68	11.98
22.80	17.96	13.98	14.97	10.76	14.98
		16.67	17.97	12.72	17.98
246.1°K		296.3°K		296.8°K	
1.15	1.00	.60	1.03	1.49	3.00
2.15	3.02	1.10	2.02	2.75	5.99
3.72	5.99	1.47	3.00	4.11	8.99
5.42	8.99	2.30	5.00	5.46	11.99
7.15	11.99	3.21	6.99	6.79	14.99
8.94	14.98	4.07	8.99	8.13	17.98
10.65	17.98	5.46	11.99		
		6.83	14.99		
		8.13	17.98		

Table 3. Experimental data for the c-axis crystal

σ	H	σ	H	σ	H
1.4°K (298°K)		4.2°K (298°K)		10.0°K (298°K)	
45.4	.19	59.97	.90	43.28	.17
49.9	.41	63.01	1.40	52.51	.41
56.0	.64	66.22	1.88	55.34	.64
59.0	.89	67.36	2.38	57.48	.90
62.16	1.39	69.54	2.87	61.32	1.39
66.11	1.88	71.40	3.37	64.57	1.88
69.87	2.87	72.89	3.87	72.21	3.87
82.17	5.85	79.76	5.86	78.73	5.86
88.67	8.84	87.75	8.84	87.06	8.84
94.57	11.83	93.99	11.83	93.64	11.83
98.98	14.82	98.83	14.82	98.69	14.82
104.8	17.88	102.40	17.82	102.50	17.82
83.41	6.1				
67.61	2.0				

σ	H	σ	H	σ	H
15.0°K (50°K)		18.3°K (50°K)		20.1°K (50°K)	
46.58	.19	38.12	.20	22.41	.46
44.09	.42	37.05	.43	33.27	.94
46.80	.66	42.62	.66	39.35	1.43
48.23	.91	43.93	.92	44.64	1.92
52.94	1.40	53.61	1.90	57.99	3.91
57.59	1.90	58.54	2.89	67.05	5.88
62.98	2.90	72.67	5.87	77.54	8.86
76.43	5.86	81.71	8.85	85.48	11.85
84.67	8.85	89.01	11.84	93.12	14.83
91.42	11.84	95.17	14.88		
96.48	14.83	99.44	17.82		
101.34	17.82				
78.21	6.1				
61.99	2.0				
53.27	1.0				

Table 3. (Continued)

σ	H	σ	H	σ	H
35.0°K (52°K)		**48.7°K (59.8°)**		**70.0°K (79.7°)**	
5.64	.99	9.81	2.98	7.65	2.99
10.90	1.98	19.26	5.97	14.86	5.97
21.47	3.96	28.46	8.95	21.93	8.96
31.00	5.94	34.37	10.94	29.11	11.95
44.23	8.92	36.01	11.44	36.38	14.93
55.38	11.90	37.55	11.93	43.44	17.92
64.98	14.89	39.04	12.43		
72.79	17.87	39.04	12.93		
		40.38	14.92		
		46.43	14.92		
		54.79	17.90		

σ	H	σ	H	σ	H
30.0°K (51°K)		**47.5°K (50°K)**		**59.8°K (50°K)**	
23.54	2.96	10.16	2.98	39.47	14.93
41.28	5.92	19.80	5.96	40.82	15.43
55.06	8.90	29.39	8.95	42.09	15.92
66.51	11.88	38.50	11.93	47.18	17.91
75.75	14.86	47.38	14.92		
83.47	17.85	55.50	17.90		

σ	H	σ	H	σ	H
25.0°K (58°K)		**40.8°K (40°K)**		**59.8°K (50°K)**	
16.35	1.00	12.47	2.98	8.30	2.98
27.59	1.95	24.29	5.96	16.01	5.97
36.65	2.93	35.45	8.95	23.88	8.96
50.10	4.91	45.66	11.92	31.72	11.94
60.08	6.89	55.45	14.90	35.58	13.44
68.08	8.88	63.84	17.89	36.86	13.93
77.98	11.86			38.24	14.47
85.57	14.85				
91.81	17.83				
69.78	9.1				
62.01	7.1				
52.22	5.2				

Table 3. (Continued)

σ	H	σ	H	σ	H
79.7°K		90.0°K		100.0°K	
7.13	2.99	6.90	2.99	6.41	2.99
13.95	5.97	13.21	5.98	12.45	5.98
20.84	8.96	19.83	8.96	18.58	8.97
27.74	11.95	26.33	11.95	24.78	11.96
34.59	14.94	32.89	14.94	30.92	14.94
41.23	17.93	39.21	17.93	36.86	17.93
39.40	15.4				
28.02	12.3				
21.25	9.1				
14.16	6.2				
110.0°K		120.0°K		130.9°K	
5.97	2.99	5.26	2.99	4.88	2.99
11.65	5.98	10.54	5.98	9.55	5.98
17.21	8.97	15.57	8.97	14.11	8.97
22.79	11.96	20.82	11.96	18.79	11.97
28.50	14.95	26.00	14.95	23.41	14.96
34.06	17.94	31.08	17.94	27.87	17.95
145.9°K		160.4°K		183.8°K	
3.78	2.99	3.16	2.99	2.80	2.99
7.57	5.99	6.20	5.99	5.12	5.99
11.35	8.98	9.42	8.98	7.59	8.99
15.13	11.97	12.69	11.98	10.15	11.98
18.85	14.97	15.76	14.97	12.64	14.98
22.52	17.96	18.78	17.97	14.99	17.97

Table 3. (Continued)

σ	H	σ	H	σ	H
217.4°K		**217.4°K**		**256.5°K**	
Run 1		Run 2		1.61	3.00
				3.05	5.99
2.08	3.00	2.02	3.00	4.54	8.99
4.02	5.99	3.99	5.99	6.04	11.99
5.90	8.99	5.86	8.99	7.57	14.99
7.85	11.99	7.77	11.99	9.06	17.97
9.77	14.98	9.69	14.98		
11.62	17.98	11.55	17.98		

295.6°K

σ	H
1.30	3.00
2.58	6.00
3.81	8.99
5.09	11.99
6.28	14.99
7.41	17.99

Table 4.   Saturation magnetic moment per gram at T°K

T°K	$\sigma_{\infty,T}$ [a]	$\sigma_{0,T}$ [b]
a-axis crystal		
1.8	306.0	-
4.2	305.8	299.3
10.0	305.8	-
12.0	305.5	298.4
14.5	305.3	297.7
19.0	304.5	297.0
22.2	304.0	296.0
24.6	303.2	295.3
<10$\bar{1}$0> crystal		
1.4	350.2	347.0
4.2	350.2	347.0
14.5	348.9	345.0
20.0	347.8	-
25.2	347.3	341.3
30.3	346.7	337.0

[a] Data obtained from Figure 10.

[b] Data obtained by extrapolation to H = 0.

Table 5.   Inverse magnetic susceptibility per gram for polycrystalline holmium

Polycrystalline sample[a]		Predicted values[b]	
T°K	1/Xg	T°K	1/Xg
140.0	0.61×10^3	136.5	0.56×10^3
170.0	0.93	145.5	0.66
200.0	1.25	185.0	1.08
230.0	1.57	299.0	2.32
260.0	1.89		
290.0	2.21		

[a] Data obtained from curves of Rhodes, et al. (9).

[b] Data obtained from single crystal values by use of Equation 5.1.

122

B. Tabulation of the Resistivity Data

Table 6. Resistivity as a function of temperature for the current flowing along an a-axis

$(\rho_{res} = 3.50 \ \mu\text{ohm-cm})$

T°K	$\rho - \rho_{res}$	T°K	$\rho - \rho_{res}$	T°K	$\rho - \rho_{res}$
77.8	29.16	168.8	67.51	4.6	0.07
81.2	31.20	179.2	69.51	5.3	0.11
87.4	34.92	185.4	70.67	6.3	0.16
92.2	37.80	197.1	72.77	8.2	0.28
97.0	40.74	207.0	74.63	10.4	0.48
102.0	43.64	216.3	76.38	12.0	0.79
106.7	46.45	226.0	78.18	14.6	1.38
111.6	49.50	235.3	79.87	16.4	1.85
116.0	52.18	249.2	82.34	18.8	2.58
121.4	55.45	206.8	84.40	19.7	2.95
124.8	57.39	272.1	86.38	20.5	3.14
126.0	58.08	285.1	88.58	21.5	3.43
127.0	58.56	296.6	90.61	22.8	3.83
128.5	59.24			24.4	4.36
129.6	59.69			26.7	5.15
130.9	60.17	138.2	61.63	29.1	6.09
132.1	60.43	133.4	60.71	32.0	7.22
133.7	60.71	131.0	60.21	34.6	8.30
134.5	60.85	129.9	59.88	34.2	8.00
136.1	61.19	129.1	59.55	38.4	9.93
137.9	61.53	127.1	58.65	46.0	13.18
139.9	61.91	125.6	57.89	51.0	15.46
144.5	62.78			55.4	17.48
149.4	63.78			60.0	19.79
159.2	65.67			62.7	21.12
				68.6	24.20
				73.3	26.65
				78.4	29.46

Table 7. Resistivity as a function of temperature for the current flowing along a <10$\bar{1}$0> direction

(ρ_{res} = 3.60 μohm-cm)

T°K	$\rho - \rho_{res}$	T°K	$\rho - \rho_{res}$	T°K	$\rho - \rho_{res}$
78.2	29.46	272.9	87.87	50.6	15.31
88.4	35.48	284.1	89.96	56.2	18.01
		296.3	92.17	59.7	19.60
				67.3	23.69
				73.3	26.86
153.2	65.04	78.3	29.58	77.9	29.42
141.2	62.62	81.5	31.57	87.5	35.14
130.2	60.31	87.2	35.28	97.6	41.25
128.3	59.56	97.8	41.83	106.8	46.88
128.3	59.54			116.1	52.54
127.0	58.93	4.3	0.09	121.6	55.82
124.8	57.76	5.3	0.07	125.0	57.87
134.1	61.21	6.3	0.07	126.2	58.49
		8.2	0.19	127.6	59.18
		10.2	0.41	127.9	59.31
141.4	62.53	12.3	0.77	129.6	60.03
148.6	63.96	15.0	1.37	130.9	60.49
149.1	64.09	16.7	1.90	132.5	60.84
159.1	66.03	19.1	2.59	133.5	61.05
169.3	68.06	19.6	2.83	135.8	61.50
179.4	69.98	20.2	3.02	138.0	61.89
189.8	72.00	21.4	3.30	140.8	62.43
199.7	74.07	22.2	3.63	144.2	63.15
212.6	76.46	24.2	4.18	150.2	64.33
212.6	76.45	25.8	4.79	155.1	65.29
225.4	78.81	27.0	5.22		
237.4	81.16	29.6	6.19		
248.8	83.37	34.9	7.99		
261.8	85.70	38.5	9.97		
272.6	87.69	43.9	12.33		

Table 8. Resistivity as a function of temperature for the current flowing along a c-axis

T°K	$\rho - \rho_{res}$	T°K	$\rho - \rho_{res}$	T°K	$\rho - \rho_{res}$
		(ρ_{res} = 3.20 µohm-cm)			
77.9	31.04	251.0	48.50	78.0	31.04
83.0	34.04	261.1	49.53	78.2	31.20
87.2	36.40	272.2	50.68	83.7	34.39
91.8	38.96	283.7	51.89	87.6	36.65
96.8	41.51	296.0	53.17		
101.6	43.58	261.4	49.57	29.0	7.30
107.0	45.44	137.8	39.79	26.8	6.37
111.4	46.50	131.7	40.28	24.3	5.43
117.2	47.11	129.2	43.16	22.4	4.75
121.4	46.76	122.8	46.41	21.1	4.31
124.8	45.81	4.3	0.08	20.2	4.05
126.0	45.27	4.6	0.13	19.2	3.68
127.1	44.69	5.3	0.17	18.6	3.42
128.4	43.86	6.3	0.20	16.9	2.71
130.8	41.35	8.2	0.36	15.5	2.09
131.7	40.33	10.1	0.65	14.4	1.64
132.8	40.10	12.7	1.24	12.9	1.24
134.1	39.79	14.6	1.79	15.5	1.95
135.2	39.74	16.3	2.32	16.8	2.43
136.1	39.73	18.7	3.29	18.7	3.16
138.2	39.77	19.3	3.63	19.4	3.51
139.1	39.73	20.0	3.95	20.1	3.92
140.2	39.74	20.8	4.25	21.0	4.23
142.0	39.76	22.1	4.69	21.6	4.41
144.6	39.81	23.2	5.08	22.2	4.65
148.2	39.92	25.0	5.68	23.2	5.00
152.0	40.08	29.0	7.26	24.2	5.37
156.4	40.32	31.8	8.42	25.2	5.75
160.3	40.61	35.1	9.82	26.5	6.23
167.5	41.00	39.4	11.71	29.0	7.27
177.5	41.74	44.0	13.80	22.2	4.69
189.2	42.69	50.5	16.42	21.5	4.46
198.8	43.50	54.7	18.68	20.7	4.25
208.0	44.34	59.8	21.20	20.5	4.16
218.4	45.32	62.0	22.42	20.3	4.09
227.6	46.18	67.5	25.32	20.0	4.01
236.7	47.11	73.1	28.29	19.4	3.74

Table 9. Resistivity for polycrystalline holmium[a]

T°K	$\rho - \rho_{res}$	T°K	$\rho - \rho_{res}$	T°K	$\rho - \rho_{res}$
		(ρ_{res} = 7.0 μohm-cm)			
1.3	0.0	30.5	6.6	129.7	51.9
2.0	0.0	32.4	7.4	131.9	51.4
3.0	0.1	35.1	8.6	135.0	52.6
3.5	0.1	38.2	9.9	141.1	52.2
4.2	0.1	41.8	11.4	150.9	53.5
13.8	1.4	49.0	14.6	162.7	55.1
15.0	1.7	55.6	17.3	176.1	56.9
16.1	2.1	64.4	21.8	189.7	60.3
17.0	2.3	71.7	25.7	200.0	60.3
18.0	2.7	77.8	29.1	210.2	61.8
18.6	2.9	82.5	31.4	221.8	63.4
19.0	3.0	92.8	37.6	233.7	64.9
19.4	3.2	103.2	43.4	246.3	66.9
19.8	3.3	114.3	48.7	263.8	69.4
20.2	3.4	120.8	51.1	275.8	70.9
21.9	3.7	124.3	51.9	284.8	72.3
27.5	5.4	127.2	52.2	297.7	74.4

[a]Data for curve published by Colvin, et al. (6).

Table 10. Predicted resistivity for polycrystalline holmium[a]

T°K	$\rho - \rho_{res}$	T°K	$\rho - \rho_{res}$	T°K	$\rho - \rho_{res}$
110.0	47.8	132.0	53.7	180.0	60.5
120.0	52.2	134.0	53.8	200.0	63.4
126.0	53.7	140.0	54.6	220.0	66.6
128.0	54.1	150.0	56.0	240.0	69.6
130.0	53.5	160.0	57.4	260.0	72.5
				280.0	75.5

[a]Data obtained by substituting values taken from single crystal curves into Equation 5.2.

C. Discussion of Errors

The estimated error in the measurement of the magnetic moment per gram is derivable from Equation 9.2 and can be expressed in the form

$$\frac{\Delta\sigma}{\sigma} = \left[\left(\frac{\Delta m}{m}\right)^2 + \left(\frac{\Delta F}{F}\right)^2 + \left(\frac{\Delta P}{P}\right)^2 + \left(\frac{\Delta g}{g}\right)^2\right]^{1/2} \qquad (9.1)$$

where $P = \dfrac{dH}{dz}$.

The estimated error in g is 0.01 per cent and is negligible. Values of m were determined on a semi-micro balance reading to 0.01 mg, and m was approximately 100 mg; so the estimated error in m is less than 0.1 per cent. Values of F ranged from 0.0060 gm at low fields and high temperatures to approximately 16.6 gm at low temperatures and high fields. With low values of F, it was possible to obtain weighings which were repeatable to $\pm$ 0.0003 gm; however, the sensitivity decreased to approximately 0.0010 when F approached 16.6 gm. The estimated error in F is from 5 per cent at low fields to 0.01 per cent at high fields.

The field gradient was calibrated by use of a field and gradient meter designed by Thoburn (66). Checks of the calibration with samples of iron, nickel and cobalt revealed that an uncertainty of slightly more than 1.0 per cent exists. Therefore, the probable error in the values of magnetic moment goes from 5.1 per cent for low F values to 1.0 per cent for high F values. Values of $\sigma_{\infty,0}$ were determined from high

F measurements; so the error in $\sigma_{\infty,0}$ is approximately 1.0 per cent.

The error in the magnetic field is about 1.7 per cent, which corresponds to 360 oersteds at the highest fields measured. Since the demagnetization correction was of this same magnitude, the error in the demagnetization correction, which is less than 10 per cent, is negligible.

Although not properly termed an error, a source of incorrect readings could be the magnetic history of the sample prior to an isothermal run. It was determined that reproducible curves could be obtained if the sample were annealed to 50°K prior to each set of measurements. It is felt that the a-axis crystal data shown in Figure 6 for 37.5°K and 45.0°K, which were obtained prior to the establishment of the annealing process, show the results of a small amount of hysteresis in the antiferromagnetic state. These isotherms were taken as part of a series -- 10°K, 37.5°K, 45°K -- with no annealing between runs. The annealing temperature prior to each isotherm is listed with the isotherm data in Appendix A.

The temperature of each isotherm was maintained by the controller described in Chapter IV, Sec. B. Temperature variations were restricted to less than $\pm$ 0.05°K. The actual temperature was determined by a copper-constantan thermocouple, and the uncertainty in temperature over the whole

temperature range is $\pm$ 0.5°K.

The resistivity was determined by the use of Equation 4.4. The estimated error in the resistivity is given by

$$\frac{\Delta\rho}{\rho} = \left[\left(\frac{\Delta V}{V}\right)^2 + \left(\frac{\Delta I}{I}\right)^2 + \left(\frac{\Delta l}{l}\right)^2 + \left(\frac{\Delta A}{A}\right)^2\right]^{1/2} \qquad (9.2)$$

A measuring current, I, of 100 milliamperes was used for all three samples. The current was controlled by 0.1 milliampere. The estimated error in current is 0.1 per cent. The potential, V, was measured with a Rubicon Type B potentiometer which could be read to 0.2 μvolt. Because of internal thermal emfs, the error in absolute value of emf is stated as 1.0 μvolt; but the smooth nature of curves of plotted data implies that the error is much less than this over short periods of time; therefore, an error 0.3 μvolt is assumed. The potentials measured varied from 15 μvolts to 490 μvolts so that errors in V ranged from 2.5 per cent to 0.2 per cent. The error in the measurement of the resistance of the sample, therefore, ranges from 2.5 per cent at low temperatures to 0.2 per cent at high temperatures.

The error in the determination of the effective length of the sample, $\frac{\Delta l}{l}$, was dependent upon the width of the marks left on the sample by the potential probes. For the a- and c-axis crystals, $\frac{\Delta l}{l}$ was estimated to be 0.2 per cent. Some difficulty was encountered in measurements on the $\langle 10\bar{1}0\rangle$ crystal. In order to obtain good contacts for the potential probes, it was necessary to fasten them more tightly than they were

fastened for the a- and c-axis crystals. The probes pressed more deeply into the sample; consequently, the marks on the sample were wider. $\frac{\Delta l}{l}$ was estimated as approximately 1.0 per cent.

The errors in the determination of the cross sectional area were approximately the same for all three samples. The error for one dimension was 1.5 per cent so that $\frac{\Delta A}{A}$ was approximately 2.1 per cent.

The total error in the form factor, $\frac{A}{l}$, for the a- and c-axis crystals was approximately 2.2 per cent, and the error for the $\langle 10\bar{1}0 \rangle$ crystal was 2.5 per cent.

In order to obtain the overall error in resistivity as given by Equation 9.2, one must combine the error in the form factor, which is temperature independent, with the error in the measurement of resistance, which is temperature dependent. The error in resistivity for the a- and c-axis crystals ranges from 3.3 per cent at low temperatures to 2.2 per cent at high temperatures. The error in resistivity for the $\langle 10\bar{1}0 \rangle$ crystal ranges from 3.5 per cent at low temperatures to 2.5 per cent at high temperatures.

Temperatures for the resistivity measurements were measured with a copper-constantan thermocouple. The calibration of the thermocouple is discussed in Chapter IV, Sec. C. Temperatures were estimated as accurate to $\pm 0.5^\circ K$ over the entire temperature range.

The crystallographic orientations for the three samples were determined to within one degree.